UNCLASSIFIED
SECURITY CLASSIFICATION OF THIS PAGE (When Data Entered)

REPORT DOCUMENTATION PAGE

READ INSTRUCTIONS BEFORE COMPLETING FORM

1. REPORT NUMBER: 16638.3-GS	2. GOVT ACCESSION NO.: AD-A095197
3. RECIPIENT'S CATALOG NUMBER: N/A	
4. TITLE (and Subtitle): Atmospheric Water Vapor: A Nemesis for Millimeter Wave Propagation	5. TYPE OF REPORT & PERIOD COVERED: REPRINT
	6. PERFORMING ORG. REPORT NUMBER: N/A
7. AUTHOR(s): Hans J. Liebe	8. CONTRACT OR GRANT NUMBER(s): ARO MIPR 30-79
9. PERFORMING ORGANIZATION NAME AND ADDRESS: Institute for Telecommunication Sciences, Boulder, CO	10. PROGRAM ELEMENT, PROJECT, TASK AREA & WORK UNIT NUMBERS: N/A
11. CONTROLLING OFFICE NAME AND ADDRESS: US Army Research Office, PO Box 12211, Research Triangle Park, NC 27709	12. REPORT DATE: 1980
	13. NUMBER OF PAGES: 59
14. MONITORING AGENCY NAME & ADDRESS (if different from Controlling Office): ARO-30-79	15. SECURITY CLASS. (of this report): Unclassified
	15a. DECLASSIFICATION/DOWNGRADING SCHEDULE

16. DISTRIBUTION STATEMENT (of this Report)

Submitted for announcement only

17. DISTRIBUTION STATEMENT (of the abstract entered in Block 20, if different from Report)

18. SUPPLEMENTARY NOTES

19. KEY WORDS (Continue on reverse side if necessary and identify by block number)

20. ABSTRACT (Continue on reverse side if necessary and identify by block number)

DD FORM 1 JAN 73 1473 EDITION OF 1 NOV 65 IS OBSOLETE

UNCLASSIFIED
SECURITY CLASSIFICATION OF THIS PAGE (When Data Entered)

403394

ARO 16638.3-GS

ATMOSPHERIC WATER VAPOR: A NEMESIS FOR MILLIMETER WAVE PROPAGATION[1]

Hans J. Liebe

U.S. Department of Commerce
National Telecommunications and Information Administration
Institute for Telecommunication Sciences
Boulder, Colorado

Millimeter waves offer an attractive way of solving unique system problems because of their ability to penetrate clouds, smog, dust or fog. This makes them a logical choice over electro-optical devices for adverse weather applications. Spectral lines of oxygen and water vapor ultimately limit the atmospheric transparency; hence, most applications operate between the absorption lines in four window regions (that is, 24 to 48, 72 to 110, 128 to 160, and 200 to 260 GHz). Observations have established the existence of excess water vapor absorption (EWA), which is most evident in these windows. Excess implies that the effect is not related to the known spectral properties of the water molecule. EWA is found to increase in nontrivial manner with humidity and the discrepancies can be as large as a factor of 10. Several groups (most notably at the Appleton Laboratory, UK), have gathered evidence of EWA from laboratory and field observations and brought forward hypotheses to account for the data. Qualitative explanations are based on the assumption that water molecules in moist air form larger molecules with a dimer being the first step in a series of stable species. Hydrogen bonding, ion attraction and attachment of the polar H_2O to foreign particles (aerosol growth) are the ordering forces considered in the clustering process. An assessment of the current EWA picture will be given and avenues of research attacks are discussed to solve the enigma in the quantitative description of the interaction between millimeter waves and moist air.

[1]*Work was partially supported by the Office of Naval Research under N00014-79-0058, and by the U.S. Army Research Office under ARO 30-79.*

ISBN 0-12-208440-3

I. INTRODUCTION

Atmospheric water in both vapor and liquid states is the major deterrent to an unrestricted exploitation of propagation of millimeter and, more so, of infrared wavelengths. For most applications, the operation of ground-based systems is limited to seven sindow regions W1 to W7, these being the gaps between molecular absorption lines and bands:

Absorption Feature	Region	Window Range
22 GHz H_2O line	W1	24 to 48 GHz
60 GHz O_2 line complex	W2	70 to 115 GHz
119 GHz O_2 line	W3	120 to 165 GHz
183 GHz H_2O line	W4	200 to 310 GHz
325 GHz H_2O line	W5	340 to 365 GHz
380 GHz H_2O line and 1823 more (H_2O rotational band)	W6	20 to 38 THz
6.3 μm H_2O band	W7	60 to 100 THz
2.7 μm H_2O band		

The main attraction of millimeter wave systems is their ability to penetrate the somewhat opaque atmosphere (haze, fog, clouds, dust, smoke, light rain) under circumstances in which electro-optical and infrared systems normally fail. Accurate and detailed knowledge of atmospheric transmission is essential to an evaluation of the advantages of millimeter waves over the shorter wavelengths.

One objective of this paper is to focus attention on unsolved problems in the construction of a valid model for atmospheric millimeter wave transmission, subject to the following conditions: Frequency, ν = 10 to 1000 GHz, with special emphasis on the EHF range, ν = 30 to 300 GHz; altitude, h = 0 to 30 km; and relative humidity, RH = 0 to $\leq$ 100%. The radio engineer uses the optical term "clear" for moist, but unsaturated air (RH < 100%), and ignores haze conditions. Although many constituents contribute to the total atmospheric attenuation rate, α (dB/km), absorption in the window is dominated by water vapor and is of greatest concern for practical situations. At present, describing water vapor absorption mechanisms and relating them to measurable quantities is partly an empirical matter and lacks credibility in a general sense.

The following interaction effects between millimeter waves and air are well documented:

Case	References
(a) Absorption line theory . . .	1, 4, 13, 31
(b) Moist air refraction	2, 5, 7, 47-50
(c) Water vapor absorption . . .	1, 3, 4, 7, 14, 16, 17, 24, 25
(d) Water vapor dispersion . . .	2, 4, 5, 7, 17, 62, 67
(e) Water vapor continuum absorption	11, 12, 18, 21, 22, 24, 26, 31
(f) Oxygen absorption	15, 17, 19, 65
(g) Complete line parameter compilation for all atmospheric molecules	110
known as the AFGL Tape, HITRAN Model and FASCODE .	10, 14, 25, 29
(h) Scattering loss by particles	33, 32, 35-37
(i) Dielectric loss of water . .	25,27, 32, 102-106

Other physical effects, which have been taken into account in infrared transmission models (9), (20), and (23) are:

(k) Submicron aerosol particles .	38, 41, 42
(l) Growth of submicron particles in moist air . .	35-37, 34

Of a more speculative nature are considerations of

(m) Water dimer $(H_2O)_2$ spectra .	6, 8, 21, 43, 58, 64, 66, 69, 81, 86, 89, 109
(n) Water cluster $(H_2O)_n$, n>2 . .	21, 22, 44
(o) Water ion activity	28, 45

The water polymer hypotheses have the inherent weakness that except for the dimer (43), neither definite structural observations have been made nor millimeter wave spectra calculated. In the cases (m) to (o), production and growth mechanisms (for example, ion-induced) as well as size and number density distributions have not been identified for the natural atmospheric environment.

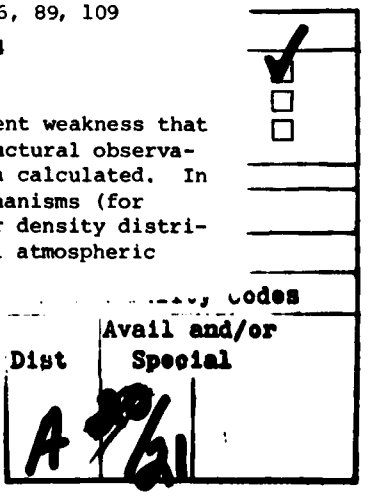

Measured absorption in the windows W1 to W7 could provide clues for the understanding of which basic physical mechanisms are missing in current models. New instrumentation, such as the dispersion spectrometer (63,65) and the saturation hygrometer (107), might prove helpful in future investigations. Available experimental results on absolute attenuation rates, path transmittances, and thermal emission from laboratory (46-71) and field (73-101) observations in cloudless moist air are generally higher than values predicted on the basis of molecular absorption alone. It is a fact, even after allowing for difficulties in measuring the highly variable water content quantitatively, that the absorption by water vapor in the atmospheric transmission windows W1 to W7 is not completely understood.

Section II of this paper presents the framework for a radio path modeling scheme of which details, such as measurements and validation, have been published (15,17,19). The model serves as a basis for the definition and discussion, in Section IV, of the problem of excess water vapor absorption (EWA) in the light of experimental data. Section III is devoted to a brief presentation of relevant physical properties of atmospheric water vapor.

II. EHF RADIO PATH MODELING

Millimeter waves traveling through the cloudless (RH $\leq$ 100%) atmosphere suffer both deterministic and random variations in amplitude and phase. Radiation is absorbed and refracted by gases and submicron particles. This interaction is modeled with the intent to predict the following frequency-dependent propagation effects: (a) absorptive loss of coherent radiation, (b) time of propagation between two points, (c) refractive ray-bending and ducting, (d) generation of incoherent noise, and (e) scintillations due to random fluctuations of the medium in space and time. The array of mathematical and empirical expressions used to compute these various effects is called the Propagation Model. Such a parameterization scheme depends foremost on spectroscopic information about kind and number density of absorber species and on their distribution within the path volume.

A. *The Propagation Model*

Complex refractivity N(ppm) is a convenient macroscopic measure of the interaction between millimeter wave radiation and the individual absorbers in moist air. A value of N accounts for the effectiveness and number density of a particular absorber population. Later these dependences are formulated in terms of measurable quantities. At this point, N is assumed to be known

and the basic relations that determine the electromagnetic behavior of a radio path are written down. The complex refractivity of a gaseous medium in ppm

$$N = N_o + D(\nu) + j\, N''(\nu) \tag{1}$$

consists of three components; namely, the frequency independent refractivity N_o plus various spectra of refractive dispersion $D(\nu)$ and absorption $N''(\nu)$. The atmosphere is characterized as a linear network with both passive and active properties. The amplitude and phase response of a plane radio wave traveling the distance L(km) and having an initial field strength E_o is described by

$$D = E_o \exp(\Gamma L) \tag{2}$$

where

$$\Gamma = j(2\pi\nu/c)(1 + N \cdot 10^{-6}) \tag{3}$$

is the propagation constant of the intervening medium, c being the speed of light. Usually, real and imaginary parts of N are separated and expressed as the power attenuation rate in dB/km

$$\alpha = 0.1820\nu IM(n) \tag{4}$$

and the phase delay rate in radian/km

$$\varphi = 0.0209\nu RE(N) \tag{5}$$

The frequency ν is in gigahertz (GHz) throughout the paper.

The attenuation rate α is the more familiar quantity in atmospheric wave propagation. The phase rate φ must be considered when it varies spatially (for example, radar pointing accuracy, long-baseline interferometry, maximum dish size for reflector antennas, etc.) or with frequency (for example, bandwidth limitations of a communication channel). Characteristics of short, horizontal radio paths may be approximated by an average value of N. More general path geometries, such as a ground-to-satellite link, are treated by dividing the path into segments having quasi-constant N-values and summing. The cummulative behavior between the ray points s_1 and s_2 is expressed in dB by the total attenuation

$$A = \int_{s_1}^{s_2} \alpha(s)\, ds \tag{6}$$

or by the transmittance (multiply by 1/10 log e + 0.023026 to convert dB to Np

$$\tau = \exp(-0.230A) \tag{7}$$

The medium becomes transparent when τ approaches one and, on the other hand, opaque for $\tau \simeq 0$.

The total phase change for the same path is given in radians by

$$\phi = \int_{s_1}^{s_2} \varphi(s)\, ds \tag{8}$$

which translates into the travel-time in ns of the wave by

$$\eta = \phi/2\pi\nu \tag{9}$$

The path differential ds is, in practice, an increment Δs over which N is quasi-constant, and depends upon the altitude, h; the starting angle, θ, from the zenith in the case of a slant path; and refractive bending of the ray (Snell's law) due to gradients $\delta\varphi/\delta s$ (19).

Absorption by the atmosphere causes emission spectra. Each unit of volume maintains thermal equilibrium with its environment via collisions; hence, the path element ds radiates an equivalent blackbody emission $T(s)\,\alpha(s)\,ds$, which is reduced by the transmittance $\tau(s)$ along the path of observation. The resulting brightness temperature in K

$$T_B = 0.230 \int_0^{\infty} T(s)\,\alpha(s)\,\tau(s)\,ds \tag{10}$$

is either less than or equal to the ambient temperature T. Equations (6), (8), and (10) constitute the key by which performance limitations of EHF systems operating over clear-air propagation paths may be evaluated. A transfer function exhibiting constant amplitue (A = constant), frequency-linear phase delay [$D(\nu) = 0$], and no noise ($T_B = 0$) implies ideal channel behavior. A broadband signal occupying a frequency interval $\Delta\nu$ is distorted by the deterministic spectra of $D(\nu)$ and $N''(\nu)$; in addition, T_B imposes detection limitations. As a bonus, the emission spectra $T_B(\nu)$ afford opportunities to sense remotely the state of the atmosphere by passive radiometric means (for example, Ref. 39 and 40).

B. The EHF Refractivity of Moist Air

The physical state of moist air is described by

dry air pressure (1 kPa = 10 mb)	P , kPa	} (11)
relative inverse temperatue (T in K)	t = 300/T	
water vapor partial pressure	e , kPa	

Calculation of the frequency-independent refractivity in ppm in Eq. (1) is straightforward (47-50)

$$N_o = 2.589\ p\ t + (41.6\ t + 2.39)\ et \tag{12}$$

Water vapor refractivity is about 16 times more effective, on a per molecule basis, than dry air in generating propagation phenomena such as delay, ray bending, ducting, scintillations, etc.

The dispersion contribution in ppm

$$D(\nu) = \Sigma_i (S\ F')_i - 41.6\ et^2 \tag{13}$$

and the absorption spectrum in ppm

$$N''(\nu) = \Sigma_i (s\ F'')_i + N''_v + N''_x \tag{14}$$

require further elaboration. Frequency-dependent molecular spectra are of two types:

1. Line spectra of absorption SF" and of dispersive refraction SF', having strength S in units of kHz and shape factors F' and F" in units of GHz^{-1}; the sums over i consider millimeter wave lines (see Tables 1 and 2) of O_2 (i = 2 to 45)[2] and H_2O (i = 46 to 74). Spectra of the trace gases O_3, CO, N_2O, SO_2, NH_3, etc., are neglected (10,17,29,31,110).

2. Continuum water vapor spectrum N''_v due to far-wing contributions of very strong infrared lines. A third term, N''_x, which is not fully understood, was added to the absorption to account for contributions other than those of the rotational water vapor line spectrum (see Section IV).

Common to each spectroscopic feature is an intensity-against-frequency distribution function, the shapes F'(ν) and F"(ν). *For h < 20 km,* the shape functions are (17)

$$F' = \left[\frac{(\nu_o - \nu) + \gamma I}{(\nu_o - \nu)^2 + \gamma^2} + \frac{(\nu_o + \nu) + \gamma I}{(\nu_o + \nu)^2 + \gamma^2}\right] \tag{15}$$

and

[2] *The nonresonant oxygen spectrum, i = 1 is discussed in Ref. 17.*

TABLE 1. Data Base for O_2^{16} Spectral Lines in Air up to 1000 GHz

i	Center frequency ν_0 GHz	Strength a_1 kHz/kPa		Temperature exponent a_2	Width a_3 GHz/kPa		Interference a_4 1/kPa		Temperature exponent a_5	ID		
1	0	3.070[a]	E-4	--	5.6	E-3	--	--	--	Nonresonant		
	50.47360	0.940	E-6	9.6900	8.60	E-3	5.200	E-6	1.79			37^-
	50.98730	2.440	E-6	8.6900	8.70	E-3	5.500	E-6	1.69			35^-
	51.50302	6.040	E-6	7.7400	8.90	E-3	5.600	E-6	1.77			33^-
5	52.02117	1.410	E-5	6.8400	9.20	E-3	5.500	E-6	1.81			31^-
	52.54223	3.080	E-5	6.0000	9.40	E-3	5.690	E-6	1.79			29^-
	53.06680	6.370	E-5	5.2200	9.70	E-3	5.280	E-6	1.89			27^-
	53.59572	1.240	E-4	4.4800	10.00	E-3	5.440	E-6	1.83			25^-
	54.12997	2.265	E-4	3.8100	10.20	E-3	4.800	E-6	1.99			23^-
10	54.67116	3.893	E-4	3.1900	10.50	E-3	4.840	E-6	1.90			21^-
	55.22136	6.274	E-4	2.6200	10.79	E-3	4.170	E-6	2.07			19^-
	55.78380	9.471	E-4	2.1150	11.10	E-3	3.750	E-6	2.07			17^-
	56.26478	5.453	E-4	0.0109	16.46	E-3	7.740	E-6	0.89	D1[b]	1^+	
	56.36339	1.335	E-3	1.6550	11.44	E-3	2.970	E-6	2.29			15^-
15	56.96818	1.752	E-3	1.2550	11.81	E-3	2.120	E-6	2.53			13^-
	57.61249	2.125	E-3	0.9100	12.21	E-3	0.940	E-6	3.76			11^-
	58.32389	2.369	E-3	0.6210	12.66	E-3	-0.550	E-6	-11.10	D2		9^-
	58.44660	1.447	E-3	0.0827	14.49	E-3	5.970	E-6	0.79		3^+	
	59.16422	2.387	E-3	0.3860	13.19	E-3	-2.440	E-6	0.07			7^-
20	59.59098	2.097	E-3	0.2070	13.60	E-3	3.440	E-6	0.49		5^+	
	60.30604	2.109	E-3	0.2070	13.82	E-3	-4.350	E-6	0.68			5^-
	60.43478	2.444	E-3	0.3860	12.97	E-3	1.320	E-6	-1.20	D3	7^+	

TABLE 1 (Continued)

i	Center frequency ν_0 GHz	Strength a_1 kHz/kPa		Temperature exponent a_2	Width a_3 GHz/kPa		Interference a_4 1/kPa		Temperature exponent a_5		ID	
	61.15057	2.486	E-3	0.6210	12.48	E-3	-0.360	E-6	5.84		9^+	
	61.80017	2.281	E-3	0.9100	12.07	E-3	-1.590	E-6	2.86		11^+	
25	62.41122	1.919	E-3	1.2550	11.71	E-3	-2.660	E-6	2.26		13^+	
	62.48626	1.507	E-3	0.0827	14.68	E-3	-5.030	E06	0.85	D4		3^-
	62.99800	1.492	E-3	1.6550	11.39	E-3	-3.340	E-6	2.18		15^+	
	63.56854	1.079	E-3	2.1150	11.08	E-3	-4.170	E-6	1.96		17^+	
	64.12778	7.281	E-4	2.6200	10.78	E-3	-4.480	E-6	2.00		19^+	
30	64.67892	4.601	E-4	3.1900	10.50	E-3	-5.150	E-6	1.84		21^+	
	65.22408	2.727	E-4	3.8100	10.20	E-3	-5.070	E-6	1.92		23^+	
	65.76474	1.520	E-4	4.4800	10.00	E-3	-5.670	E-6	1.78		25^+	
	66.30206	7.940	E-5	5.2200	9.70	E-3	-5.490	E-6	1.84		27^+	
	66.83677	3.910	E-5	6.0000	9.40	E-3	-5.880	E-6	1.74		29^+	
35	67.36951	1.810	E-5	6.8400	9.20	E-3	-5.600	E-6	1.77		31^+	
	67.90073	7.950	E-6	7.7400	8.90	E-3	-5.800	E-6	1.73		33^+	
	68.43080	3.280	E-6	8.6900	8.70	E-3	-5.700	E-6	1.65		35^+	
	68.96010	1.280	E-6	9.6900	8.60	E-3	-5.300	E-6	1.74		37^+	
39	118.75034	9.341	E-4	0.0000	15.92	E-3	-0.441	E-6	0.89			1^-
40	368.49835	6.790	E-5	0.0200	15.60	E-3	0	--	---		$1,3^-$	
	424.76312	6.380	E-4	0.0112	14.70	E-3	0	--	---		1,3	
	487.24937	2.350	E-4	0.0112	14.70	E-3	0	--	---		$1,3^+$	

TABLE 1 (Continued)

i	Center frequency ν_0 GHz	Strength a_1 kHz/kPa		Temperature exponent a_2	Width a_3 GHz/kPa		Interference a_4 1/kPa		Temperature exponent a_5	ID
	715.39315	9.960	E-5	0.0891	14.40	E-3	0	--	---	$3,5^-$
	773.83873	5.710	E-4	0.0798	14.00	E-3	0	--	---	3,5
45	834.14533	1.800	E-4	0.0798	14.00	E-3	0	--	---	$3,5^+$

[a] Units: ppm/kPa

[b] D denotes doublet

TABLE 2. Data Base for H_2O^{16} Spectral Lines in Air up to 1000 GHz

l[a]		Center frequency ν_0 GHz	Strength b_1 kHz/kPa	Temperature exponent b_2	Width b_3 GHz/kPa		ID (lower quant. no.) (10)			References
46		22.235080	0.105	2.143	28.1	E-3	5	2	3	(7,56,57)
		68.052000	0.002	8.750	28.0	E-3	4	1(1)[b]	4	(10)
	•	183.310091	2.380	0.653	28.2	E-3	2	2	0	(51,55,13)
		321.225644	0.046	6.160	22.0	E-3	9	3	6	(10,13)
50	•	325.152919	1.550	1.520	29.0	E-3	4	2	2	(10,13)
	•	380.197372	12.300	1.020	28.5	E-3	3	2	1	(10,13)
		386.778000	0.004	7.330	16.0	E-3	11	2	10	(10,110)
		437.346670	0.063	5.020	15.0	E-3	6	6	0	(10,13)
		439.150812	0.921	3.560	17.5	E-3	5	5	0	(10,13)
55		443.018295	0.191	5.020	14.8	E-3	6	6	1	(10,13)
	•	448.001075	10.700	1.370	24.6	E-3	3	3	0	(10,13)
		470.888947	0.328	3.570	18.1	E-3	5	5	1	(10,13)
		474.689127	1.240	2.340	21.0	E-3	4	4	0	(10,13)
		48 .491133	0.256	2.810	22.2	E-3	7	1	7	(10,13)
60		504.219000	0.038	6.690	12.7	E-3	7	7	0	(10,110)
		505.126000	0.012	6.690	13.0	E-3	7	7	1	(10,110)
	•	556.936002	526.000	0.114	31.7	E-3	1	0	1	(10,13)
	•	620.700807	5.210	2.340	21.6	E-3	4	4	1	(10,13)
		658.340000	0.460	7.760	32.8	E-3	1	0(1)	1	(10)
65	•	752.033227	259.000	0.336	30.2	E-3	2	0	2	(10,13)
		836.836000	0.012	8.110	17.0	E-3	11	2	9	(10,110)
		859.810000	0.015	7.990	27.0	E-3	2	0(1)	2	(10)
		899.380000	0.091	7.840	30.0	E-3	1	1(1)	1	(10)

TABLE 2 (Continued)

i[a]		Center frequency ν_0 GHz	Strength b_1 kHz/kPa	Temperature exponent b_2	Width b_3 GHz/kPa		ID (lower quant. no.) (10)			References
		903.280000	0.064	8.350	28.0	E-3	2	2(1)	1	(10)
70		907.773000	0.179	5.040	20.4	E-3	8	3	5	(10,110)
	•	916.169000	8.900	1.370	24.9	E-3	3	3	1	(10,110)
	•	970.320000	9.400	1.840	24.6	E-3	4	3	1	(10,110)
	•	987.940000	145.000	0.180	29.9	E-3	1	1	1	(10)
74	•	1097.368000	840.000	0.656	33.5	E-3	3	0	3	(10,110)
Plus 1809 additional lines up to 31 THz, of which 361 lines have strengths, $b_1 > 1000$. The strongest lines are at:										
	•	2774.100000	2023.000	0.208	29.5	E-3	1	1	0	Max. strength
	•	6076.500000	2500.000	1.370	20.4	E-3	3	3	0	Max. attenuation

[a] Continued from Table 1.

[b] (1) denotes 1. vibrationally excited state.

• Stronger lines.

$$F'' = \left(\frac{\nu}{\nu_o}\right)\left[\frac{\gamma - (\nu_o - \nu)\, I}{(\nu_o - \nu)^2 + \gamma^2} + \frac{\gamma - (\nu_o + \nu)\, I}{(\nu_o + \nu)^2 + \gamma^2}\right] \qquad (16)$$

introducing the spectroscopic parameters of center frequency ν_o, width γ, and overlap interference I. F' and F" are in units of 1/GHz.

For h > 20 km, only isolated resonant lines are present, spread over a megahertz frequency scale. Equations (15) and (16) reduce to Lorentzian shapes

$$F'_L = (\nu_o - \nu)/[(\nu_o - \nu)^2 + \gamma^2] \qquad (17)$$

and

$$F''_L = \gamma/[(\nu_o - \nu)^2 + \gamma^2] \qquad (18)$$

where F'_L and F''_L are in units of 1/GHz. Peak dispersion at $\nu = \nu_o \pm \gamma$ and maximum absorption at $\nu = \nu_o$ are given in ppm by

$$\pm D_m = S/2\gamma$$

$$N''_m = S/\gamma \qquad (19)$$

For h > 40 km, a further decrease in pressure converts the pressure-broadened Lorentzian into a Doppler-broadened Gaussian shape with a different width in kHz of

$$\gamma_D = 6.20\, \nu_o/\sqrt{mt} \qquad (20)$$

where m is the molecular weight (e.g., O_2, m = 32, t = 1, ν_o = 60 GHz: γ_D = 65.8 kHz).

The convolution of Lorentzian and Gaussian shape functions is called the Voigt profile, which is governed by the parameter γ/γ_D. The Voigt profile is appropriate when this ratio falls in the range between ≃ 10 and 0.1. Numerical evaluation of the height-dependent complex Voigt function requires considerable computational effort (19).

1. Microwave Spectrum of Oxygen (O_2-MS). The O_2 molecule has electronic, vibrational, and rotational energy levels with transitions causing spectral lines from the optical to the EHF range. The EHF lines are fine structure transitions between rotational triplet energy levels. All pertinent information on the O_2-MS is tabulated; that is, the line parameters have been reduced to five coefficients a_1 to a_5, which are listed in

Table I together with the center frequencies ν_o (17,19). Dependence on atmospheric properties is expressed by

$$S = a_1\, p\, t^3 \exp[a_2(1 - t)] \tag{21}$$

$$\gamma = a_3\, (p + 1.3e)\, t^{0.9} \tag{22}$$

$$I \simeq a_4\, p\, t^{a_5} \tag{23}$$

where S and γ are in kHz and GHz, respectively. Water vapor influences the O_2-MS through Eq. (22).

2. Microwave Spectrum of Water Vapor. From the AFGL line parameter compilation (10), 1838 H_2O lines were read up to 31 THz when a maximum intensity ($\nu = \nu_o$) cutoff of 2×10^{-3} dB/km (300 K) is applied. For the EHF range, 29 lines (see Table 2) must be considered explicitly and the remaining ones are lumped into a continuum far-wing contribution. An individual line is described by

$$S_v = b_1\, e\, t^{3.5} \exp[b_2(1 - t)] \tag{24}$$

$$\gamma_v = b_3(p + 4.80\, e)t^{0.6} \tag{25}$$

$$I_v = 0$$

where S_v and γ_v are in kHz and GHz, respectively.

3. Continuum Water Vapor Spectrum. The remaining 1809 (that is, 1838 - 29) H_2O lines make far-wing contributions; they are fitted by (17)

$$N''_{v,i} \simeq 1.9 \times 10^{-5}\, p\, e\, t^4\, (\nu/30) \tag{26}$$

The continuum absorption N''_v in ppm is of a magnitude and functional form that is similar to the empirical Gaut-Reifenstein expression (11)

$$N''_v \simeq 5.6 \times 10^{-5}\, p\, e\, t^{3.1}\, (\nu/30) \tag{27}$$

which was introduced by Waters (31) and has proven useful to other workers (32,108). The far-wing contributions to refractivity of all rotational H_2O lines yield with Eq. (12) in Eq. (13) the term $41.6\, et^2$ (3,4,5). The contribution of the local lines, i = 46 to 74 to this value is in ppm

$$\sum_i (SF'(\nu \to 01)_i \simeq 4.75\, et^3 \tag{28}$$

Very accurately measured refractivity can serve as a test for the low frequency response of theoretical line shapes applied to the rotational H_2O spectrum if one is sure of the spectroscopic data base. A more detailed discussion of Eqs. (26) and (27) follows in Section IV.

4. Temperature Behavior. A closer look at the spectral line response aids in understanding the temperature dependence of EHF attenuation and phase dispersion rates in moist air. Line intensities are sensitive to temperature variations at various rates. The peak line intensities in ppm (Eq. (19)) are described by

	S/γ
O_2	$(a_1/a_3)[p/(p + 1.3e)]\ t^{2.1}\exp[a_2(1 - t)]$
H_2O	$(b_1/b_3)[e/(p + 4.8e)]\ t^{2.9}\exp[b_2(1 - t)]$

(29)

The line intensities are independent of temperature when

		t = 1.1	1.3	1.5	2
O_2	$a_2 = 2.1\ell n\ t/(t - 1)$	2.00	1.87	1.70	1.46
			(see Table 1)		
H_2O	$b_2 = 2.9\ell n\ t/(t - 1)$	2.76	2.54	2.35	2.02
			(see Table 2)		

(30)

Lines with values lower than those prescribed by Eq. (30) increase in intensity when the temperature drops ($t > 1$) and vice versa. A useful approximation at a fixed frequency is given by

$$\alpha(t) = \alpha(300\ k)\ t^{y} \tag{31}$$

where the exponent y is obtained by fitting model data.

C. The Radio-Path Model

The path is assumed to be in a spherically stratified atmosphere in which each layer is homogeneous. The integral expressions (Eqs. (6), (8) and (10)) are evaluated by the *layer-by-layer* method (19,29) by using numerical integration techniques since closed-form solutions are lacking because of the complicated temperature height profile.

Mean conditions are modeled by the U.S. Standard Atmosphere 1976, and in situ data from radiosonde ascents can be programmed in directly. Whatever description of the atmosphere is employed, model or data, it is converted in the computer into n-layers

each having an assigned set of values of p(h), e(h) $\leq e_s$, t(h). Values for α are calculated by using Eqs. (4), (14), (16) and (21) to (25) and for φ by applying Eqs. (5), (12), (13,) (15) and (21) to (25), by the standard *line-by-line* superposition (29) and adding the continuum Eq. (27).

The radio path is assumed to be a ray (that is, plane wave case), and the general procedure is to calculate the local N(h) (1) for the programmed altitude grid reporting p, e, t and to store N_o, D(ν), and N"(ν) separately on file. The ray starts at a surface height h_o with an elevation angle θ and is guided through the inhomogeneous medium until it reaches the intended fianl height h_1. Refraction is most pronounced at the lowest heights and causes substantial ray bending when θ is close to 0° (tangential path); thus, many fine steps are required initially.

Modeling is introduced for the purpose of predicting the mean of EHF propagation effects and the limits of their variability from readily available climatological data bases. In order to apply such a tool in an optimum manner, it is important to consider the uncertainties in the spectroscopic data and the limitations imposed by the numerical calculation procedure.

D. Typical Examples

The examples presented in Figs. 1 to 7 almost speak for themselves. Figure 1 is a presentation of the complete rotational water vapor spectrum for a typical sea-level condition. It was calculated by using the AFGL Data Tape (10) rather than the EHF model given in sections B and C, and serves to demonstrate the very strong (over 6 orders of magnitude) absorption due to water vapor in the far-infrared that allows on the low frequency end just a few eindow ranges for transmission.

A more refined modeling result is depicted in Fig. 2. It displays at higher altitudes (h = 16 km) spectral signatures of the trace gases O_2, CO, N_2O, which are not included in the described model. At tropospheric heights (h = 0 and 4 km), only lines of H_2O and O_2 (see markings at bottom of figure) are important. The figure gives, in essence, a picture of atmospheric molecular absorption in the millimeter and submillimeter wavelength range. These computations by Burch and Clough (24) agree well with reported data and the presented model (Eqs. (27) and (4)) of the water vapor continuum spectrum labeled α_x. The attenuation rate spans seven orders of magnitude over the frequency range ν = 100 to 1000 GHz and altitudes h = 0 to 16 km where > 99.5% of the atmospheric water vapor is contained. The transparency in the window ranges W2 to W5, which are valleys between the absorption line peaks, is dominated by the water vapor continuum α_x. Figure 2 affirms the dominant role that

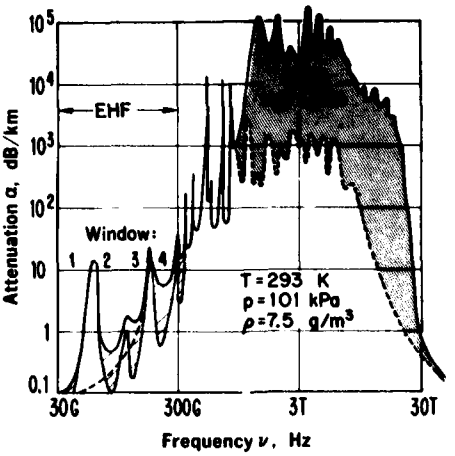

FIGURE 1. Attenuation rate α at sea level (h = 0 km, e = 1.015 kPa) over the frequency range, ν = 30 GHz to 30 THz displaying the envelope for maximum/minimum values of the rotational water vapor spectrum. Calculated by using the AFGL Tape (10).

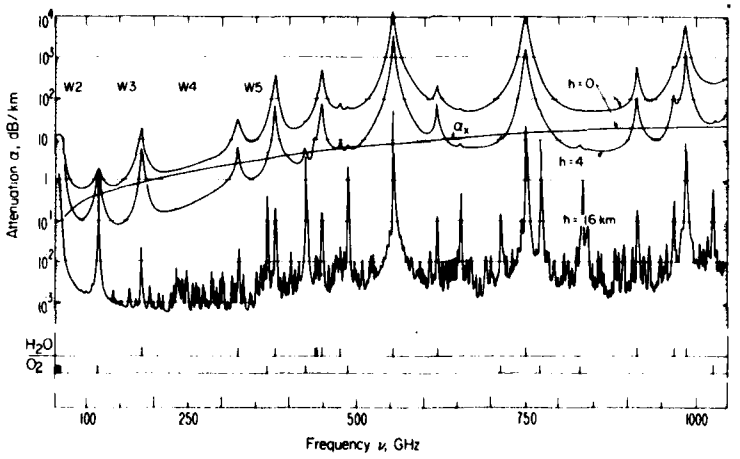

FIGURE 2. Attenuation rate α at the altitudes, h = 0, 4, and 16 km over the frequency range, ν = 100 GHz to 1000 GHz. The following atmospheric conditions and trace molecular number densities $M(m^{-3})$ were used in the calculation (24):

h,km	p,kPa	t	e,Pa	$M(O_3)$	M(CO)	$M(N_2O)$
0	101.0	1.041	786.000	6.78E17	1.91E18	7.12E18
4	61.6	1.144	133.000	5.77E17	1.28E18	4.76E18
16	10.4	1.385	0.061	3.01E18	2.59E17	9.67E17

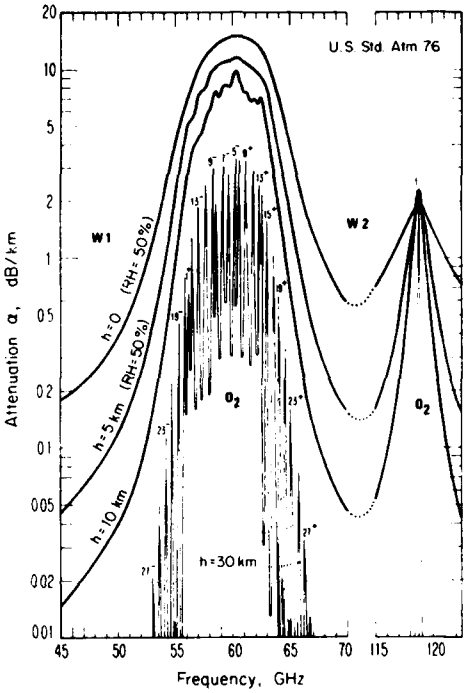

FIGURE 3. Attenuation rate α at the altitudes, h = 0, 5, 10, 30 km over the frequency range, ν = 45 GHz to 125 GHz displaying band and line structure of the oxygen microwave spectrum.

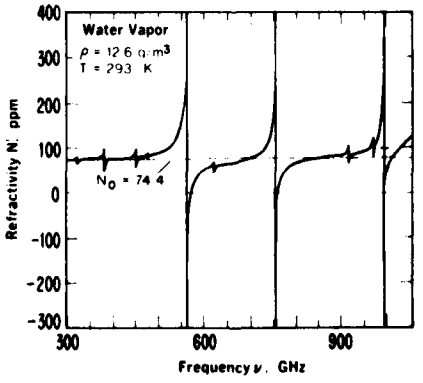

FIGURE 4. Pure water vapor refractivity N_O + D(ν) for e = 1.705 kPa over the frequency range, ν = 300 GHz to 1000 GHz from measurements and calculation (67).

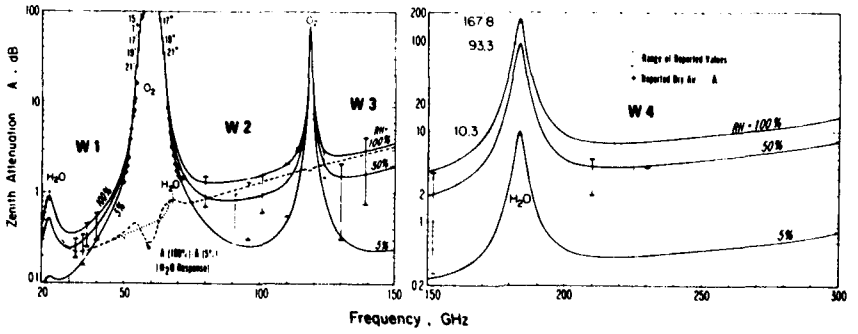

FIGURE 5. Zenith attenuation A through the first 30 km of the U.S. Standard Atmosphere 1976 for dry (RH = 5%), moderate (50%), and humid (100%) air over the frequency range, ν = 30 GHz to 300 GHz (EHF). The relative humidity RH was assumed to be constant for h = 0 km to 8 km (19). The experimental data are from Ref. 80 and Table 5.

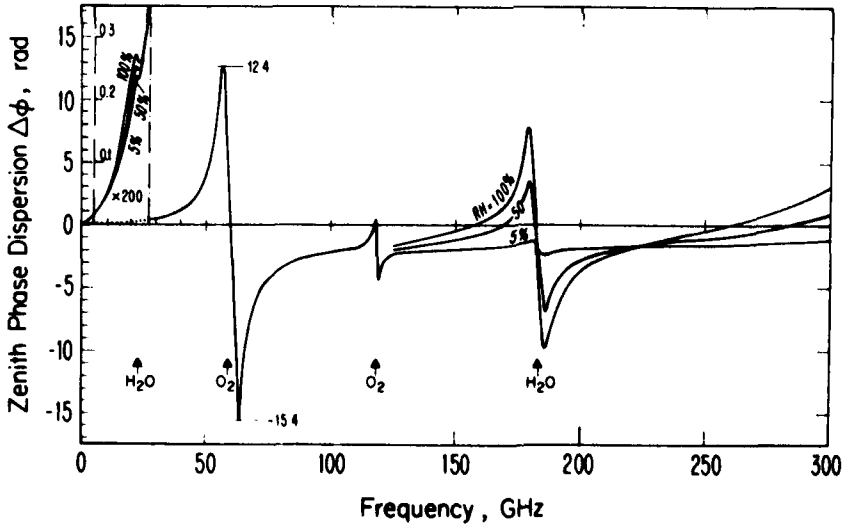

FIGURE 6. Zenith phase dispersion $\Delta\phi = \phi - \phi_o$ (Eq. (18)) for the same conditions specified in Fig. 5. The frequency-independent delay time due to $\phi_o[N_o(h)]$ is (Eq. (9)):

RH,%	*5.000*	*50.000*	*100.000*
η,ns	*7.666*	*7.977*	*8.266*

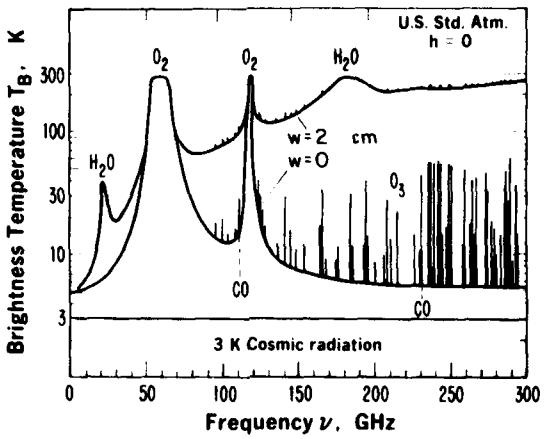

FIGURE 7. Zenith brightness temperature (atmospheric noise) T_B downwelling to ground from a dry (w = 0) and a moist (w = 2 cm, Eq. (33)) air mass (31).

water vapor absorption plays in atmospheric millimeter wave propagation, even at modest humidities (RH = 46% for h = 0).

A more detailed picture of molecular attenuation appears in Fig. 3. The oxygen microwave spectrum dominates in the ranges 50 to 70 GHz and 115 to 123 GHz. At levels close to the surface, the 60-GHz lines are merged into an unstructured band shape, the maximum intensity of which is pressure-proportional, until the lines separate (h > 15 km). Above 15 km, the shielding effect breaks down and radio channels with up to 400 MHz bandwidth can be accommodated between the lines. If there is a line close to the frequency of interest, isolated line behavior takes over. In the frequency-agile applications, it is possible to tune to a more or less constant shielding factor (for example, 0.5 dB/km) over the height range h = 0 to ≃ 30 km. Above h > 30 km, Zeeman splitting has to be considered in the frequency intervals $\nu_o \pm 5$ MHz until the O_2 lines vanish above h > 100 km (19).

It is encouraging to the author to see experimentally verified results on millimeter wave water vapor refractivity expressed by $N_o + D(\nu)$, an example of which is presented in Fig. 4. After many careful measurements of microwave refractivity in the fifties and sixties (2,3,5,47-50,56), this marks a new start in a heretofore inaccessible frequency range. In comparison with conventional absorption spectroscopy, refractive dispersion measurements are superior for absolute intensity studies (15,57,65). An important result of Fig. 4 is the fact that the much stronger lines beyond

1000 GHz determine, by means of their far-wing intensity, most of the microwave refractivity N_o (see Eq. (28)).

E. Cumulative Behavior

A standard example for an inhomogeneous medium is the one-way zenith response through the U.S. Standard Atmosphere 1976 (19). Figures 5 and 6 display the cumulative attenuation A and cumulative phase dispersion $\Delta\phi$, for which 48 height levels up to h = 30 km are summed. Except for the vicinity ($\nu_o \pm 10$ MHz) of the O_2-MS lines, these curves represent the one-way zenith path behavior. Three humidity profiles $\rho(h)$ were used to model RH = 5, 50, and 100% in each of 26 height layers between h = 0 and 8 km. The RH drops rapidly below 1% above h = 8 km. The frequency range 55 to 65 GHz is opaque (A > 30 dB) for any system attempting to look through. The transmittance, Eq. (7) is measurable when the atmosphere is somewhat transparent (A < 30 dB), and it can be determined either by the absorption of a signal coming from the outside (sun emission, satellite beacon) or by the thermal emission originiating predominately in 8 km thick layers. Frequencies around 57 and 63 GHz yield the maximum and minimum phase dispersion for the 60-GHz band, which is almost independent of the water vapor content. Actually, the foreign-gas broadening of the O_2-MS by water vapor (see Eq. (22)) reduces the attenuation slightly with increasing vapor pressure (see Fig. 5: A(100%) - A(5%)). Comparison of the total attenuation A with measurements (see Table 5) yields reasonably good agreement when the empirical assumptions formulated by Eq. (27) are used in the calculation. The amount of water vapor absorption for a given atmospheric condition can be estimated, to some extent, if the surface vapor concentration ρ_o is known.

The EHF thermal emission by H_2O, O_2, O_3 and CO was calculated by Waters by using Eqs. (10), (7) and (4) and the absorption coefficients given in Eq. (31). Calculations are shown in Fig. 7 both for no water vapor and for a total precipitable water vapor of 2 cm. The integral is evaluated for h = 0 to 60 km. Clear-sky emission varies primarily with the amount of water vapor. The calculations are for observations in the zenith direction from ground level. Cosmic radiation of 3 K, which is incident on the atmosphere from the top, has been added to Eq. (10).

III. PHYSICAL PROPERTIES OF ATMOSPHERIC WATER VAPOR

The clear atmosphere appears in the EHF radio path modeling scheme only as a p-t-e (Section II, B) parameter system. The real atmosphere is an enormous theater of diverse but related and incessant activities (33). Water, endlessly changing its phases, is the main actor on this stage. On a global scale,

each year about 1 m of the ocean depth is evaporated, whereas the average water content of the atmosphere represents a depth of roughly 2 cm. Water vapor is rapidly exchanged causing it to be a patchy, capricious medium with parcels (scale sizes, 10 to 100 m), blobs (< 0.5 m) and strata ($\simeq 1$ m) of moisture that probably account for a fair share of the scatter and inconsistencies in millimeter-wave propagation data taken from field observations. The total integrated water vapor and liquid water in a vertical column can be detected with high time resolution (≥ 10 s) by ground-based radiometry in the microwave range (40). In relating millimeter-wave propagation and atmospheric water vapor, one has to be generally content to make predictions with no more than statistical certainty.

The fact that the three phases of water contribute to the weather cycle at the prevailing conditions (p-t-e) is most fundamentally a consequence of the molecular structure of H_2O. Water molecules tend to associate through hydrogen bonds[3] having about one-tenth the strength of a molecular bond. Very schmatically, in the solid phase four H-bonds form a rigid lattice; in the liquid phase, on the average, two H-bonds amalgamate chainlike links; and in the gaseous phase, a chance exists to associate singly H-bonded molecules to dimers (21,43, 44) or aggregate into clusters of preferred sizes (that is, 10 to 50 molecules) (22,28) under the influence of ion-activity (45). If further notice is taken that atmospheric air is never free from invisible particles having a variety of origins, chemical compositions, sizes, and affections for water vapor, then the radio engineer will almost despair at the prospects of ever putting order in the atmospheric pandemonium. The value of the interdisciplinary Workshop on Atmospheric Water Vapor for providing guidance with this task must be stressed.

A. Absolute Humidity

The amount of water vapor (that is, absolute humidity ρ), present in the atmosphere depends upon: (a) evaporation from surfaces; (b) transport by motions on various scales, mainly through the troposphere; (c) condensation-forming clouds and fog that causes precipitation fallout. The radio propagation engineer measures the amount of water vapor by means of an average concentration $\bar{\rho}$, which varies at sea level between the extremes of 0.1 (dry, winter, polar) and 60 g/m^3 (wet, summer, tropical). The height distribution is approximated from a known ground level ρ_o by

[3]*The electron-rich end of O in the polar molecule H_2O attracts an electron-poor H end of a neighbor H_2O.*

$$\rho(h) = \rho_o \exp(-h/2 \text{ km}) \tag{32}$$

and the most realistic measure for predictions is the total precipitable water vapor in cm (10 $g/m^3/km$ = 1 cm).

$$w = \int_{s_1}^{s_2} \rho(s)\, ds \approx 0.2\, \rho_o \tag{33}$$

The quantity w is measured, for example for a zenith path, with a microwave radiometer (39,40). The variations of the dry air parameter p(h) and t(h) are described by standard height profiles and attention is called to the model of the U.S. Standard Atmosphere (for example, (33)). The number density for the atmospheric gases with constant volume mixing ratio (O_2, N_2, CO_2, noble gases; or referred to as dry air) follows directly from the p-t combinations. Over the height range h = 0 to 16 km, the changes are for p from 101 to 10 kPa (1 kPa = 10 mb) and for t from 0.9 (333 K) to 1.5 (200 K). Ozone (O_3), besides water vapor, has a variable mixing ratio which is modeled separately. Examples of O_3 millimeter wave spectra are shown in Figs. 2 and 7 as reported by others.

Fractional fluctuations due to water vapor paths and turbulence are typically in the ranges

$$\left.\begin{aligned} \delta\rho &= \pm\ 80\% \\ \delta t &= \pm\ 1\% \\ \delta p &= \pm\ 0.1\% \end{aligned}\right\} \tag{34}$$

Variability of humidity for a midlatitude location with a medium of 7.4 g/m^3 is diurnally ± 1.0, seasonally ± 6.3, and locally ± 1.2 g/m^3.

1. Molecular Quantities. The molecular world of sea level air is very empty. The molecular radius r ≈ 1.8 x 10^{-4} μm, average spacing d, and average distance ℓ between collisions are in the radios r : d : ℓ = 1 : 18 : 320 (33). Most of the time, a molecule is unperturbed by neighboring molecules. The number of dry air molecules per unit volume (m^{-3}) is

$$M_d = 2.415 \times 10^{23}\ pt \tag{35}$$

(e.g., p = 101, t = 1 : M_d = 2.44 x 10^{25}).

Water vapor is an imperfect gas. From thermodynamic measurements, it is known that there are slightly more H_2O molecules

per unit volume than predicted by the ideal gas law. The correction is made by introducing the second virial coefficient B(t). The molecular number density of H_2O for a given vapor concentration (in g/m^3)

$$\rho = 7.219\ e\ t \tag{36}$$

follows from the relationship in m^{-3}

$$M_v = [(2.989/\rho)\ 10^{-23} + B(t)]^{-1} \approx 3.346 \times 10^{22} \tag{37}$$

(e.g., $\rho = 10 : M_v = 3.35 \times 10^{23}$).

Very few values for B(t) have been reported (44,69):

t	0.9	1	1.2
T, K	333	300	250
B, $10^{-27} m^3$	-2.8	-1.9	-0.9

The deviations from ideal behavior

$$\varepsilon = [M_v/M_v^o\ (B = 0)] - 1 \tag{38}$$

are small, even at saturation (see Eq. (43)):

t	0.9	1	1.2
$\rho = \rho_s$, g/m^3	130	25.5	0.82
ε, 10^{-3}	12.3	1.6	0.03

The deviation ε led to the postulation of a dimer molecule $(H_2O)_2$. The molecular structure (43) and the millimeter wave spectrum of the dimer (6,8,69) are well established; however, its number density under tropospheric conditions is not known.

The dimer number density is expected to depend strongly on temperature since the hydrogen bond strength is rather weak. Data which are suspected to be caused by a dimeric effect can be analyzed for their percent change-per-degree or for their power law (t^Y) dependence to allow a positive identification:

Data % Change/K	y	eV/molecule	kcal/mole	
-1.56	3.8	0.1	2.31	
-2.54	7.7	0.2	4.60	←H-bond
-3.78	11.6	0.3	6.90	
-6.22	19.3	0.5	11.60	
-12.10	39.0	1.0	23.10	←Condensation

Bond strength is expressed in units of eV/molecule or kcal/mole and the value expected for a hydrogen bond lies between 3 and 5 kcal/mole. The dimer number density in m^{-3} was proposed to follow an expression (6)

$$M_D = M_v^2 \cdot k(t) \tag{39}$$

An approximate equation in m^3 for k(t) was derived from expressions given by Bohlander (69)

$$k \approx 1.8 \times 10^{-27}\ t^{5.6} \tag{40}$$

which when combined with Eqs. (37) and (39), yields in m^{-3}

$$M_D \approx 2.0 \times 10^{18}\ \rho^2\ t^{5.6} \tag{41}$$

and for the fractional dimer concentration

$$M_D/M_v \approx 6.1 \times 10^{-5}\ \rho\ t^{5.6} \tag{42}$$

(for example, $\rho = 20$, $t = 1$: $M_D/M_v \approx 1.2 \times 10^{-3}$).

Other estimates on the fractional dimer concentration M_D/M_V are reported in Ref. (21): 0.4×10^{-3} for $\rho = 20$ assuming 5.4 kcal/mole; and in Ref. (44): 1.9×10^{-3} at $t = 1$ and 0.95×10^{-3} at $t = 1.11$, when extrapolated from saturated water vapor data taken over the range $t = 0.77$ to 0.84. These ratios M_D/M_v are close to values of ε defined in Eq. (38).

B. Relative Humidity

The examples of atmospheric millimeter wave propagation (Figs. 1 to 7) showed clearly the dominant influence of water vapor. Some difficulties in predicting this influence obviously are related to the fact that water vapor is a vapor and not a gas. The first consequence of the vapor state is that a maximum concentration ρ_s cannot be exceeded. A balance exists between two states called the saturation point. At saturation, the rate at which molecules evaporate from a plane surface (liquid or

solid) equals the rate of incoming condensing molecules. The saturation concentration over water for atmospheric conditions is fitted by

$$\rho \leq \rho_s = 17.39\ t^6\ 10^{(10-9.834t)} \tag{43}$$

in g/m^3 and is in a very rough approximation simply in g/m^3

$$\rho_s \approx 25\ t^{-17} \tag{44}$$

Equation (43) is programmed into the radio path model (Section II), which uses RH(h) information to calculate with t(h) the values e or ρ.

The saturation concentration defines relative humidity

$$f = \rho/\rho_s \approx 0.04\ t^{17} = 0.28\ et^{18} \leq 1 \tag{45}$$

or, in the more familiar percent notation, RH - 100f $\leq$ 100%. The maximum vapor concentration varies over a wide range as a function of temperature.

T, K	t	t^{-17}	ρ_s(true)[a]	ρ_s, Eq. 43	ρ_s, Eq. 44
333.30	0.900	6.000	130.350	130.400	150
300.00	1.000	1.000	25.500	25.500	25
273.16[b]	1.098	0.203	4.850	4.840	5
250.00	1.200	0.045	0.822	0.822	1

[a] Smithonian Hydrometric Table (see (33)).

[b] Triple Point

The interdependences between RH, ρ, w, and T are shown in Fig. 8. The humidity condition RH = 100% is a delicate balance point for phase changes. A drop in temperature by 1 K decreases the water vapor density of saturated air by about 6%. Energy is released during condensation which was stored in the random motion of H_2O molecules. One cubic meter of a forming cloud that converts 1 g of vapor into the liquid phase releases 2.5 kJ.

The latent heat release can generate electric fields. Depending upon the suddenness, the amount of cooling, and the water vapor supply, more or less violent updrafts (such as cumulonimbus clouds in thunderstorms) feed a turbulent air motion. Small aerosols are lofted into the upper region of a

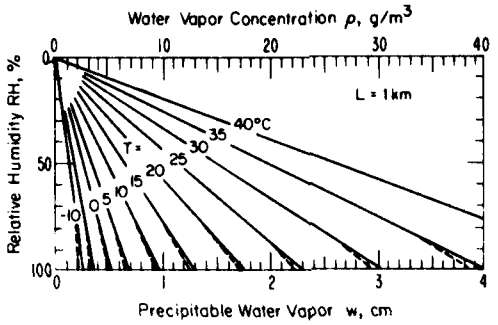

FIGURE 8. The amount of precipitable water vapor w in a radio path of length, L = 1 km and the corresponding homogeneous water vapor concentration ρ, both as a function of relative humidity RH for various temperatures T. The temperature dependence of saturation water vapor pressure e_s and maximum vapor concentration ρ_s (RH = 100%) (33) is:

T, C	e_s, kPa	ρ_s, g/m³
-30	0.051	0.453
-20	0.125	1.070
-10	0.286	2.360
0	0.611	4.840
10	1.227	9.390
20	2.337	17.270
30	4.243	30.310
40	7.378	51.020

The broken lines indicate schematically the range where water uptake by aerosol takes place (Fig. 9).

forming cloud while the larger, heavier ones remain suspended at lower levels. The small aerosols carry a positive charge, the lower levels take on a negative charge. The charge separation generates high electric field strengths and lightning discharges occur when a value of about 30 MV/m is reached. Even before, additional ions must be produced, which are suspected to have catalytic influence on the formation of homomolecular cluster $(H_2O)_n$ with n ≃ 10 to 50 (28).

C. Submicron Hydrometeors

Atmospheric air is never free from invisible particles (aerosols) having a wide variety of origins, sizes, and chemical composition, and most importantly, having the ability to convert water vapor into submicron hydrometeors. To account for aerosol activity, one must follow the evolution of particle size spectra

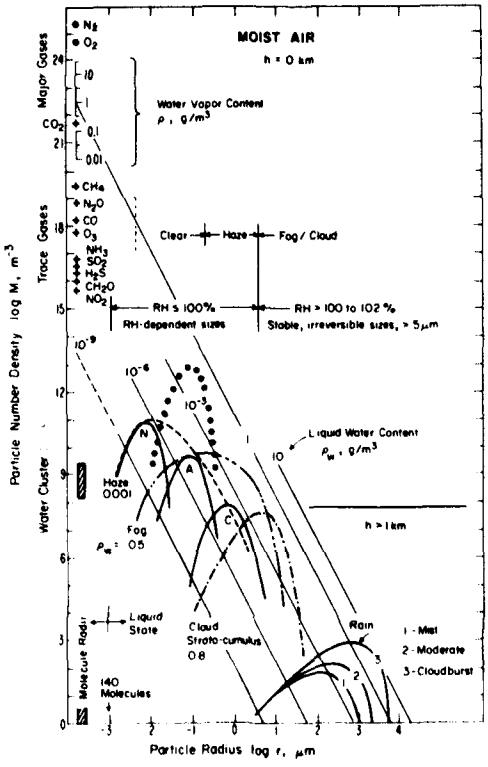

FIGURE 9. Schematic size distribution of number density M for equivalent spherical atmospheric particles from molecular to rain drop sizes, r = 10^{-4} to 10^{4} μm (32,33,41).

and the attendant microphysical processes of mass transfer over many orders of magnitude in size ($r \simeq 2 \times 10^{-8}$ to 1 cm) and number density ($M \simeq 10^{23}$ to 1 m^{-3}). This problem of scale is sketched in Fig. 9 to illustrate the extent of the difficulties. The amount of relevant literature dealing with aerosols is overwhelming and the referenced material (33-45) is probably an incomplete selection in the search for nonmolecular millimeter wave absorbers in moist air.

Aerosol models start from dry particles, distributed over three distinct size ranges (Fig. 9) (35-38): N, nucleation mode; A, accumulation mode; C, coarse particle mode; and X, hypothetical submicron distribution required to explain EWA (see Section IV). Each mode is described by representative values of a

log-normal distribution (23,43). A major process for the formation of the N-mode is the trace gas-to-particle conversion. Sulphur dioxide, for example, nucleates with water vapor to form sulfuric acid primary particles in large numbers (as high as 10^{15} m^{-3}), which are rapidly (within ms) coagulated by Brownian motion into the N-mode (34). This mode may contain sizable mass concentrations, $\rho_A(N) \lesssim 20$ $\mu g/m^3$ (38), but more to the point, it presents an enormous surface area S_A to the vapor phase and enables the aerosol to respond quickly to changes in relative humidity RH. Particle number density M_A and total surface area S_A for 1 mg of water distributed in spherical droplets of radius r with 1 m^3 are related as follows

	r, μm	M_A, molec/m^3	S_A, cm^2
N	0.01	2.4×10^{14}	3000
A	0.10	2.4×10^{11}	300
C	1.00	2.4×10^{8}	30

(46)

The mixture of gas and suspended particles is called an aerosol.

Solution droplets, such as H_2SO_4, are highly hygroscopic; that is, they adapt their size by taking up water if the RH in the ambient air is larger than the equilibrium RH over the droplet's surface. In a reverse situation, their size will shrink because of evaporation. Other hygroscopic agents are salt particles found in maritime (NaCl) as well as in urban [for example, $(NH_4)_2SO_4$] environments. These crystals undergo a sudden phase transition to become solution droplets at critical RH values (RH = 76% and 80% for NaCl and $(NH_4)_2SO_4$, respectively). The aqueous particles, or so-called hydrometeors, collect in stable, RH-dependent sizes predominantly in the A-mode. A third type of aerosol particle is relatively passive dust grains in sizes commensurate with the A and C modes. The solid matter accumulates a film of water on its surface. All the particle population is able to aggregate water (CN) but the small, hygroscopic parts of the CN (CCN) play the dominant role.

The total aerosol mass concentration in air with a humidity of ρ = 1 g/m^3 can range from ρ_A = 1 (clean air) to 400 $\mu g/m^3$ (polluted). At RH = 50%, an average mass loading of about 0.1 mg/m^3 has been deduced from data collected at 291 locations in the U.S. (38). Values between 0.5 (clean air) and 3 mg/m^3 (polluted) are reported for ρ_A in cloud free aerosol (42).

Water vapor-to-liquid conversion becomes effective when RH exceeds 80%. An aerosol population can triple, even quadruple its dry state size, and thus lead to more than a hundred-fold increase in mass concentration. Since the average size stays below 1 μm, a more or less invisible cloud exists, optically

categorized in the atmosphere as haze. Optically active sizes (> 0.5 μm) in sufficient number are only produced if the limit RH = 100% is exceeded. In that case, the available amount of water (for example, that due to a sudden cooling of saturated air) is shared either by many (> 10^9) active particles (CCN) and small (r ≃ 8 μm), uniform droplets form as fog or cloud, or by very few (< 10^8) and large (r > 100 μm), destablizing droplets that produce rain.

The water uptake of aerosol has a theoretical foundation in the relationship between the ambient RH and the equilibrium radius of a particle. Hänel provided empirical data on the hydrometric activity of aerosol (35). He defined a mass growth factor g(f = RH) with respect to the dry mass concentration ρ_A° and measured in the laboratory the equilibrium growth behavior of typical air samples. Two examples are depicted in Fig. 10. The accretion of water to particles is substantial when RH exceeds 80% and gives them almost pure water properties; that is, $\rho_A(f > 0.8) = \rho_w$. Two approximate expressions for g(f) can be formulated (35)

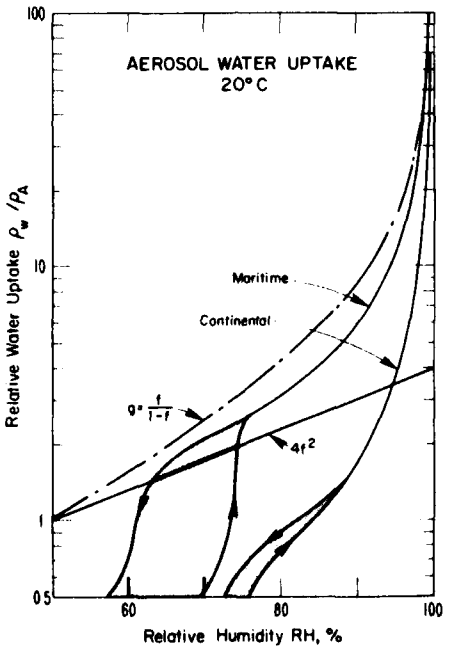

FIGURE 10. Water uptake [mass growth factor g(f = RH)] of two representative aerosol samples [maritime: NaCl; Continental: $(NH_4)_2SO_4$ + SiO_2] as a function of increasing and decreasing relative humidity RH (35).

$$g(f) \simeq 4f^2 \quad (f < 0.8) \tag{47}$$

and

$$g(f) \simeq 1/(1-f) \quad (f < 0.95) \tag{48}$$

if differences and hystereses in the growth behavior due to the chemical makeup are disregarded. A detailed discussion of models for growth factors can be found in Refs. 36 and 37.

By referring to radio path modeling, it is possible, at this point, to formulate a path-integrated liquid water content in mm

$$W = \int \rho_w \, ds = \int \rho_A^\circ \, g(f) \, ds \simeq \int [\rho_A^\circ/(1-f) \quad ds \tag{49}$$

The water content W increases at the expense of the precipitable water vapor w defined by Eq. (33); hence, in cm

$$w(f) = w(f=0) - W \tag{50}$$

The amount of liquid water in moist air (RH $\leq$ 100%) is difficult to measure. Several indirect methods have been developed. Three more promising techniques are

1. The mass concentration ρ_A° of a dried air sample is determined by micro-weighing and available (35) empirical growth factors g(f) are applied. For example, at RH = 99%, the values for g range between 65 and 120 and yield W = 0.013 to 0.024 mm when ρ_A° = 0.2 mg/m^3 over a path length L = 1 km.

2. A passive, radiometric microwave method measures at two (or more) difficult frequencies the sky noise T_B (see Eq. (10) and Refs. 39 and 40). The brightness temperature T_B is converted into zenith attenuation A (dB) by means of the spectroscopic data base. Guiraud et al. (40) perfected the technique, which uses an instrument operating at 20.6 and 31.65 GHz. The retrieval algorithms for the simultaneous determination of water vapor and water liquid content are adjusted to take into account a priori statistics (that is, a representative radiosonde profile). For example, the climatology of Oklahoma City yielded (40) in cm

$$w = 6.22\ A(20) - 2.72\ A(31) - 0.01$$

and in mm (51)

$$W = 1.30\ A(31) - 0.53\ A(20) - 0.001$$

The frequency 20.6 GHz is close to the 22 GHz vapor line (Table 2) and responds mainly to vapor; the frequency 31.65 GHz is remote from the line and responds to the dielectric loss of water. This instrument provides around-the-clock monitoring of w and W.

A typical record over 7 consecutive days (Oklahoma City, April, h = 360 m, locking at zenith) displayed for each 24-hour period the following extremes (40):

Day	w, cm	W, mm
1	2.5 to 1	0.01 to 0.02
2	1 to 2.6	0.02 to 0.5
3	2.4 to 0.8	0.02 to 2
4	1 to 2	0.03 to 1.5
5	0.5 to 1.2	0.1
6	0.8 to 1.3	0.1
7	2.4 to 4.2	0.1 to 1.5

The point of this example is that the low limits of W usually exceed the values that are obtained when using an average dry aerosol mass concentration and assumed g(f)- factors. The high limits of W are most likely due to visible clouds since their size range (r = 7 to 100 μm) contains the bulk of the water. Unfortunately, the data were not accompanied by notes providing information or meteorological or optical conditions. A similar, satellite-borne radiometer yields, over ocean surfaces with well-defined emission temperatures, the same information on w and W on a global scale (39).

3. The measurement of optical transmission gives insight into the average aerosol state. Both the optical (λ = 0.55 μm) attenuation rate α_μ and the visibility V = 20 dB/α_μ are related to the liquid water content ρ_w. In general, Mie scattering theory has to be applied in order to predict values of α_μ based on available size distributions and the complex refractive index of the particle material (23,33,35).

For the purpose of this paper, it is surficient to bypass the elaborate, lengthy calculations and discuss the main features with the help of a simple empirical expression (27,37)

$$\alpha_\mu \simeq 300\ \rho_w^{0.6} \qquad \text{or} \qquad V \approx 0.067/\rho_w^{0.6} \tag{52}$$

where α_μ is in dB/km and V is in km. The relationships between α_μ, V, and the path-averaged water content $\bar{\rho}_w$ are approximately:

ρ_w , g/m^3 ..	< 0.001	0.01	0.05	0.1	0.5
α_μ , dB/km.	< 5	19	50	75	198
V , km ...	> 4	1.1*[1.5]	0.4*[0.5]	0.27*[0.3]	0.10*[0.08]
	Clear	Haze , RH $\leq$ 100%		Fog, RH > 100%	

*[ ] = experimental value

Frequently, haze and fog conditions are described merely by stating the measured value of the visibility V* which, however, depends on the definition of the threshold value [20 dB for L = 1 km in Eq. (52)]. Nilsson performed detailed Mie calculations on five different aerosol models with the result that visibility V (16 dB threshold) and relative humidity RH are related directly (23). The range of RH for these models is

V , km	50	15	5	2
RH, %	20 to 73	84 to 95	96 to 99	98.7 to 99.7

In summary, the salient points of this section are:

1. The physical foundations for path-averaged water vapor w (Eq. 33) and liquid water content W (Eq. 49) were traced in measurable quantities. Both are expected to be the main source for millimeter wave absorption in moist air.

2. The number density M of the major molecular absorbers was given for O_2 in Eq. (35), for H_2O in Eq. (37), and for $(H_2O)_2$ in Eq. (41).

3. The water-vapor-to-water-droplet conversion in atmospheric aerosol and the associated scale problems were discussed to aid in the comprehension of the stages that a water molecule has to undergo before precipitating out of the atmosphere. The key role of relative humidity RH (Eqs. 43 to 48) in this process was underlined.

4. The interdependence between the optical properties (Eq. 52) of moist air and the liquid water content is not unique; it depends strongly on the aerosol size distribution.

IV. EXCESS WATER VAPOR ABSORPTION--EWA

Water vapor absorption (Eq. 14) in the millimeter wave windows stems from the fact that the intensity of the local millimeter wave lines $N''_\ell = \Sigma SF''$ (Table 2) is insignificant and that two other absorption terms, N''_v and N''_x, become dominant.

The far-wing response N''_ν of the rotational spectrum of H_2O beyond 1000 GHz (Fig. 1) is estimated by applying the approximation $\gamma << \nu << \nu_o$ to the line shape F" (Eq. 16) and results in

$$F''_\nu \approx 2\gamma\nu/\nu_o^3 \tag{53}$$

where F''_ν is in units of 1/GHz. The H_2O far-wing continuum of *one* line in ppm follows with Eqs. (24), (25), (53), and (11) as

$$N''_\nu = SF''_\nu \approx C_\ell(1.50\ p\rho\ t^{3.1} + \rho^2\ t^{2.1})\nu \tag{54}$$

where

$$C_\ell = 0.184\ b_1\ b_3/\nu_o^3 \tag{55}$$

For moist air, the ρ^2-term due to self-broadening is always smaller (< 20%) than the foreign gas-broadening term $p\rho$. The far-wing contribution of the strongest H_2O line (Table 2: ν_o = 2774 GHz, $C_\ell = 5.14 \times 10^{-10}$) is for an atmospheric condition described by p = 100 kPa, t = 1.023 (20°C), ρ_s = 17.27 g/m^3, at the frequency ν = 300 GHz, $N''_\nu = 4.77 \times 10^{-4}$ ppm or α_ν = 0.026 dB/km, to which the ρ^2-contribution is 11%. The line center attenuation rate, in comparison, is $\alpha_m = 7.40 \times 10^5$ dB/km. Most certainly, line shape theory (Eq. 16) is overtaxed when it is applied to predict relative intensities in the far-wing over seven orders of magnitude.

An unspecified term N''_x was added to Eq. (14) to account for discrepancies between predictions based on summing N''_ν-terms (54) and measurements. The only certainty in the conflicting evidence for N''_x is its correlation with atmospheric humidity. The abbreviation EWA (excess water vapor absorption) is used to describe N''_x. For simplicity's sake, different, mostly exponential temperature functions have been reduced to a power law t^y (Eq. 31). In this section, the exponents of physical (ρ^x, t^y) and frequency (ν^z) dependences are formulated for absorption models and compared with those for experimental data. This procedure appears to be one practical way of identifying a specific absorption mechanism, especially since EWA observations are not overwhelmingly consistent.

Two schools of thought have evolved to explain EWA:

1. A molecular approach searching for water polymers $(H_2O)_n$ and their spectra in the atmosphere. Sizes of n = 2 (dimer)[42] (6,8,21,69,81,86,89) and n = 3 (cluster) (21,28) are possibilities.

[4] *Jona already in 1919 had considered a water dimer to explain anomalous dielectric water vapor results (72).*

2. Liquid water uptake by submicron aerosol particles under conditions of high relative humidity (RH > 85%) (9,20,23,25,30, 35).

Each conjecture is supported by some *as well as contradicted by other* bits and pieces of experimental evidence.

A. Definition of EWA

Window attenuation, both model and experimental, is fitted to expression in dB/km of the form

$$\alpha = 0.182\nu N'' = C\, p^x\, t^y\, (\nu/30)^z \qquad (56)$$

where x, y, z are the proper exponents of a particular absorption model.

The AFGL compilation lists 38 350 H_2O lines from 20 GHz to 331 THz (10) ordered in seven bands (14), of which 1809 rotational lines up to ν = 13 THz contribute to the millimeter wave continuum (17). A fit to these results yielded Eq. (26), which can be reformulated into Eq. (56). Magnitude and exponents for the line continuum are given in dB/km/g/m^3/kPa by

$$C_v \approx 8.4 \times 10^{-6}$$

and (57)

$$x_v = 1.2$$

$$y_v \approx 3$$

$$z_v \approx 2$$

These exponents are based on the molecular number density (Eq. 37) displaying the exponents x = 1 and y = 1. With Eqs. (56) and (57), it follows for the sample conditions above (ν = 300, p = 100, ρ = 17, t = 1.023) that α_v = 2.75 dB/km.

The dimer spectrum is discussed in detail in Refs. 69 and 109. Absorption should follow dependencies given by Eq. (57), but modified for the dimer number denisty (Eq. 41). The response predicted in this fashion in dB/km/(g/m^3)^2 is

$$C_D \approx \text{(value of Table 4)}$$

and (58)

$$x_D = 2$$

$$y_D \approx 8$$

$$z_D = \text{values of Table 4}$$

Aerosol liquid water attenuation is obtained from published dielectric data on bulk water (Fig. 13) yielding in dB/km in the Rayleigh approximation [$\varepsilon' = (n_w')^2 + (n_w'')^2$, $\varepsilon'' = 2n_w'n_w''$] (25,30, 32).

$$\alpha_A \simeq 0.82\nu p_w \varepsilon''/[(\varepsilon' + 2)^2 + (\varepsilon'')^2] \quad (59)$$

Another method of calculating the aerosol liquid water attenuation assumes that the medium has a refractive index $n_A' \simeq 1$, and that the attenuation in bulk water is increased due to wavelength shortening ($\lambda_w = \lambda_o/n_w'$). This allows to formulate

$$\alpha_A \simeq (\alpha_w/n_w') \ (W/L) \quad (60)$$

Both methods have been applied to the latest dielectric data on water (106) producing somewhat different values (see Table 4). Frequency and temperature dependencies, when approximated using Eq. (60), follow in dB/mm from the rough data fit

$$\alpha_w/n_w' \simeq 24 \ (\nu/300)^{0.65} \ t^{-6}$$

Now, if the liquid water content is estimated by Eqs. (49), (47), and (45), $W \simeq 6 \times 10^{-3} \ L \ \rho^2 \ t^{34} \ \rho_A^o$, one obtains for the expected aerosol response in the form of Eq. (56) that

$$x_A \gtrsim 2$$

$$y_A \simeq 28$$

$$z_A \simeq 0.65 \quad (61)$$

In summary, millimeter wave window attenuation α might very well be a combination of up to five different contributions:

$$\alpha = \alpha_\ell(\text{local lines}) + \alpha_v(\text{far-wings}) + \underbrace{\alpha_A + \alpha_D + \alpha_x(\text{cluster?})}_{\text{EWA}} \quad (62)$$

A parametric study of water vapor concentration (ρ) and temperature (t) dependencies could, in principle, reveal the following behavior in the attenuation rate:

T °C	ρ_s, g/m^3	ρ_s^2, (g/m^3)^2	Multiplication factor with respect to 300 K data: t	t^3 Eq. (57)	t^8 Eq. (58)	t^{28} Eq. (61)
-20	1.07	1.15	1.185	1.664	3.890	116.00
-10	2.36	5.57	1.140	1.482	2.850	39.00
0	4.84	23.34	1.098	1.324	2.110	14.00
10	9.39	88.20	1.060	1.191	1.590	5.10
20	17.27	298.30	1.023	1.071	1.200	1.90
30	30.31	918.70	0.990	0.970	0.923	0.76

Data obeying $x \simeq 1$ and $y \simeq 3$ but displaying magnitudes different from C_v (Eq. 57) can be interpreted as failure of the line shape function (Eq. 16) to predict far-wing intensities. Discrepancies of this nature will be most pronounced for dispersion intensities (Eq. 15). Wing data of $D(\nu)$ drop more gradually ($\propto 1/\nu$) with decreasing frequency, and actually blend into the well-known refractivity N_o (Eq. 12) for $\nu < 100$ GHz, as seen in Fig. 4.

B. Excess Water Vapor (EWA) Evidence from Laboratory Data

Laboratory measurements play an important role in verifying modeling schemes for EHF properties of moist air. Generally, all the spectroscopic parameters (> 200) entering into Eq. (1) should be deduced from absolute intensity measurements under well controlled ν-p-t-ρ conditions. By a judicious choice of the experimental variables, it is possible to investigate most parameters separately.

Numerous millimeter wave and infrared studies of water vapor and moist air have been reported. References 46 to 72 are selected for their bearing on the EWA problem. Evidence for EWA from these efforts is summarized in Table 3. It is not limited to absorption, but also shows up in dispersion spectra $D(\nu)$ (63) and in refractivity N_o-studies (48,49,52,56,63). The experiments are performed by various techniques. The radio path is simulated in an enclosure either for a single-transit or a multiple-reflection (resonator) passage. Detection sensitivity increases with path length. The transmitted energy can be a single frequency, a frequency pair for differential measurements, or a broadband (Fourier transform) signal. Main variables for an experiment are either frequency or pressure, the latter being

TABLE 3. Summary of Laboratory Studies of Continuum H_2O Absorption

Continuum H_2O absorption					Experimental conditions				
Frequency ν, GHz	x (ρ)	y (T)	z (ν)	Foreign gas	H_2O density ρ, g/m^3	Temperature T, K	Path length or L, m	Resonator Q, x 10^3	Ref.
18-31	1,2			Air	0-40	318		800(Q-box)	46
22	2			N_2	0-50	312		45	56
22,24	1,2				0-20	297	(30)	16	63
31,62	1,2	2,10	2		0-35	280-325	(>100)	>200	63
117-120	>1				0-25	295	150		74
170-300	2				0-20	295		100	53
213	2	4,26		N_2	0-60	270-320	(40)	Q-box	66
210-300	2	>10			3-6	273-333	28		58
450-960					1	295	2		59
890,965	1,2				0-35	293,323	10-60		58
300-1500			0.5			290-355	5-103	and Q-box	69
9-18THz						283,329	133		69
12-36T	1,2								12
14-27T	1,2	>10			2-20	293-313	500		60
21-38T	1	5.5			14	296-388	1185		54
28-33T	1,2	2,16	2	N_2,O_2	0-20	289-301			70
75-86T	1,2				14	298	21		68

preferable for EWA studies. Gas mixture control and vacuum reference are laboratory advantages for absolute intensity studies.

Water vapor is recognized to be a medium that is difficult to control, even in the laboratory, due to its attractive force toward surfaces. The surface area of the laboratory enclosure replaces, in a way, the micro-surface of an atmospheric aerosol population. Water molecules do not ordinarily aggregate spontaneously, but water vapor becomes liquid water when wettable surfaces are present to retain the impinging molecules. A threshold of $> 2 \times 10^{-5}$ cm^{-1} in the surface-to-volume ratio is sufficient to form a continuous interface between vapor and liquid (38). This value is always exceeded in atmospheric air (see Eq. 46) as well as in a laboratory test chamber. An experimenter can select surface materials that, to a certain extent, passivate the attraction for water vapor. A systematic study was made of various surface coatings applied to an electropolished stainless steel (SS 304) cavity (3440 cm^3 and 1265 cm^2, $S/V = 0.37$ cm^{-1}) evacuated for > 24 hours to 10^{-4} torr and subjected to pure water vapor, $e_o = 2.40$ kPa at 23.0°C. Results on the relative amount e/e_o of water-uptake by the walls and the time response of the absorption (η_{Ad}) and desorption (η_{De}) process are as follows:

Coating	e/e_o,%	No.[b]	η_{Ad},s	η_{De},s
Teflon FEP120 (DuPont), 1 coat	-1.00	20	180	500
SS 304, electropolished	-1.50	30	150	400
HMDS[a] silanizing	-1.35	27	190	750
Parylene C (Union Carbine)	-1.60	32	140	580
Silicone SR240 (GE)	-2.10	42	200	550
Teflon REP120, 2 coats	-2.90	58	230	5500
Clear lacquer	-4.00	80	300	7200
60 GHz spectrometer cell, untreated (63)	-19.5(!) ($S/V = 1.28$ cm^{-1})	102	2 hrs	5 hrs

[a]Hexamethylidisilazane $[(CH_3)_3Si]_2NH$
[b]Number of molecular layers

The need for minimum S/V-ratios and judicious material selection for laboratory enclosures is clearly evident upon comparing the performance of one of the typical spectrometer cells with the preceding test. Water vapor surface effects have been recognized (52); yet, in many cases (46,49,56), they were excused as a possible source of error for the reported data. Work close to saturation requires a circulating gas-handling system with controlled mixing and continuously monitored RH levels (107). Additional sources of error are disturbances in thermodynamic

equilibrium: (a) the vapor heats up when injected into an evacuated cavity, (b) the absorption process releases heat and vice versa, (c) the ambient gas temperature is lowered during pump-down. All laboratory results on spectroscopic data (N_o, D, N") of water vapor should be seen in light of these comments. Some selected examples displaying EWA behavior are discussed in the following.

1. Moist Air Studies. Llewellyn-Jones et al. (66) investigated the temperature dependence of the frequency ν = 213 GHz by studying moist nitrogen (p = 93 kPa) over the range T = 270 - 320 K. The attenuation (Eq. 62) for these conditions can be described by the empirical expression in dB/km

$$\alpha = 0.22\rho t^2 + 0.01\rho^2 t^4 + 0.03\rho^2 t^{26} \qquad (63)$$

Close to saturation, the following values result from Eq. (63):

T, K	t	ρ, g/m^3	α, dB/km
250	1.20	1	0.32 + 0.02 + 3.43 = 3.8
273	1.10	5	1.33 + 0.37 + 8.94 = 10.6
386	1.05	10	2.43 + 1.22 + 10.67 = 14.3
300	1.00	20	4.40 + 4.00 + 12.00 = 20.4

2. Pure Water Vapor Studies. In the case of self-broadening an exponent x = 2 (Eq. 54) is expected. Mrowinski (56) observed $\alpha_x \simeq 3 \times 10^{-4}\ \rho^2$ dB/km at ν_o = 22.235 GHz and T = 39°C, in addition to the line absorption α_ℓ. Measurements by Liebe (63) at 30.6 GHz and 61.2 GHz, T = 300 and 325 K yielded in dB/km

$$\alpha \simeq 4 \times 10^{-3}\rho t^2 (\nu/60)^2 + 8 \times 10^{-4}\rho^2 t^{10} (\nu/60)^{2.5} \qquad (64)$$

The same experiment gave for the refractive dispersion (ppm), D = N'(61.2) - N'(30.6), the result

$$D \simeq 2 \times 10^{-3}\rho t^8 + 1.2 \times 10^{-3}\rho^2 t^{16} \qquad (65)$$

which is an average of the type of result exhibited in Fig. 11. The dispersion response resembles the water uptake curves (see Fig. 10) published by Hänel (35) and provided the impetus for the discussion presented in Section III.*C*.

Bohlander experimented extensively in the 100 GHz to 1000 GHz range and deduced from attenuation data, including results from other investigators, the component α_x/ρ^2 shown in Fig. 12 and listed in Table 4 (69, 109). He also calculated (by theoretical

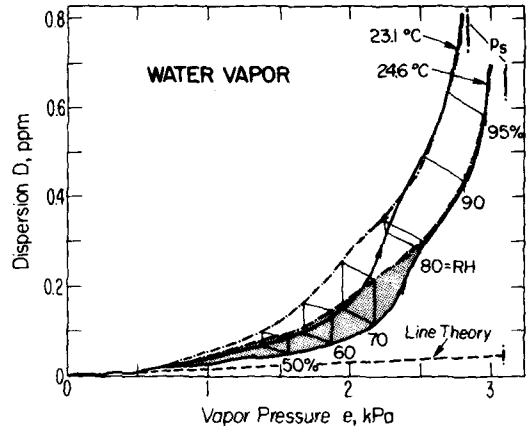

FIGURE 11. Dispersion D of pure water vapor measured with a spectrometer cell between the frequencies 61.2 and 30.6 GHz (63). A strong anomalous component is displayed exhibiting a condensation/evaporation hysteresis typical for water uptake activity (see Fig. 10).

means) the envelope of a rotational dimer spectrum, a fractional dimer concentration (Eq. 42) of 10^{-3} being assumed. The data fit between EWA and the dimer attenuation (c/x in Table 4) is poor; the spectral shapes do not match. The fit is much improved if the aerosol attenuation rate (Eqs. 59 and 49) in dB/km

$$\alpha_A = (\alpha_w / n_w') \rho_w \tag{66}$$

is used in the comparison (a/x in Table 4). Equation (66) assumes pure liquid water droplets of submicron size. Actually, based on this fit, it is possible to predict a liquid water concentration ρ_w that is needed to reproduce the EWA data of Table 4; that is, in g/m^3

$$\rho_w \simeq 1.1 \times 10^{-3} \rho^2 \tag{67}$$

At this point, the reader might recollect the arguments that have been brought forward to formulate Eqs. (47), (49), (59), and (61). Millimeter wave attenuation by submicron hydrometeors is derived from Mie's scattering equations in the Rayleigh approximation (33). The refractive index and attenuation rate of bulk water are presented in Fig. 13 (102-106). The bulk water attenuation α_w is higher because of refractive wavelength shortening in the medium; hence, the division by n_w' is applied for the gaseous aerosol medium ($n' = 1$).

TABLE 4. The EWA Component α_x/ρ^2 Reported in Refs. 69 and 109 Compared with the Water Dimer Spectrum α_D/ρ^2 Calculated by Bohlander (69) and with the Aerosol Liquid Water Attenuation (a,b).

Attenuation	Code		Frequency ν, GHz										T, °C	Ref.	Fig.
			100	200	300	400	500	600	700	800	900	1000			
α_x/ρ^2	x	+)[a]		19	26	32	37	42	46	50	52	55	23	69	12
α_D/ρ^2	c	+)[a]	4	10	18	45	50	40	25	15	11	7	23	69	12
α_A/ρ_w		*)[b]													
(Eq. 59)	b		4	9	16	21	26	31	36	40	43	46	25	25, 32, 106	
(Eq. 60)	a		7	16	23	28	33	38	42	45	48	51	25	106	
			H_2O--Attenuation Rate												
Data	a/x			0.84	0.88	0.88	0.89	0.90	0.91	0.90	0.92	0.92			
	b/x			0.47	0.62	0.66	0.70	0.74	0.78	0.80	0.83	0.84			
Fit:	c/x			0.53	0.69	1.41	1.35	0.95	0.54	0.30	0.21	0.13			

[a] +) Units: $[dB/km/(g/m^3)^2] \times 10^{-3}$.

[b] *) Units: $dB/km/g/m^3$.

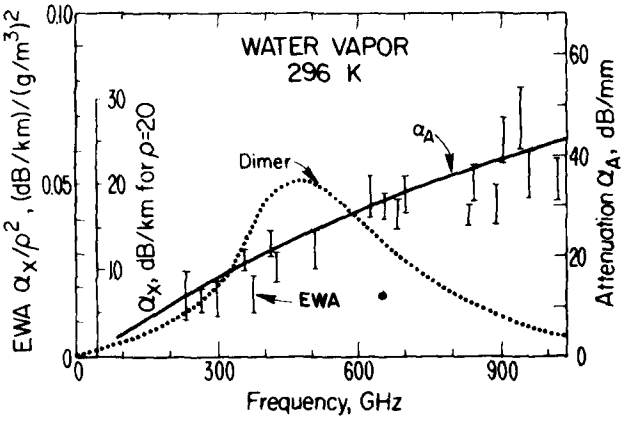

FIGURE 12. Summary of reported frequency dependence for excess water vapor absorption, compared with a rotational dimer band spectrum ($M_D/M_V = 10^{-3}$) (69) and the absorption spectrum α_A of liquid water in submicron hydrometeors (see Table 4).

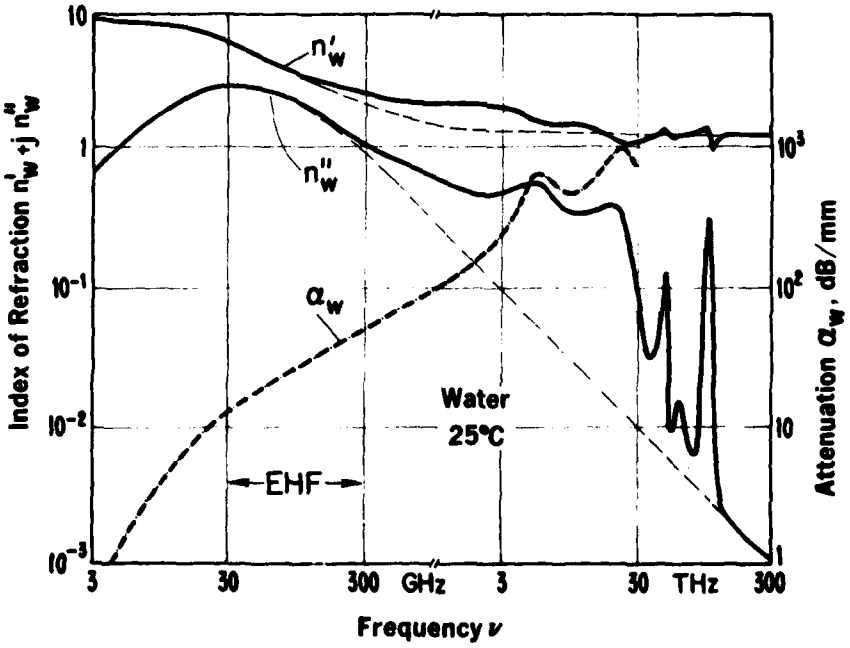

FIGURE 13. Complex refractive index n_w and bulk attenuation rate α_w of water as a function of frequency, ν = 3 GHz to 300 THz (composite from Refs. 102 to 106).

TABLE 5. Summary of Reported EHF Radio Path Attenuation and Comparison with Model Calculations

(a) Horizontal Path at Sea Level[a]

	Model (19)		Field data[b]			
RH,%	0	100[c]	0	100[c]	Water vapor data fit	Ref.
ν, GHz	α, dB/km		α, dB/km		ρ, g/m^3	
80.000	0.010	0.56	--	0.510	0.04(2)ρ	81
130.000	0.020	1.28	--	1.540	0.12(3)ρ	81
171.000	0.010	4.93	0.200	4.800	$0.375\rho + b\rho^2$	77
250.000	0.000	4.57	--	4.900	0.38ρ	101
304.000	0.000	8.16	0.000	41.000	3.2ρ	75
337.000	0.000	16.89	0.600	18.400	$0.8\rho + 0.05\rho^2$	100
345.000	0.000	13.50	0.000	8.400	$0.45\rho + 0.016\rho^2$	89
350.000	0.000	14.00	--	17.900	1.4ρ	101

(b) Zenith Path from Sea Level[a]

	ν, GHz	A_d, dB	A, dB	A_d, dB	A, dB	ρ_o	(A_v) or	w, cm	Ref.
	15.000	0.050	0.11	0.055	0.106	0.004ρ			31
	15.000	0.050	0.11	0.046[b(a)]	0.085[b(b)]	0.003ρ			91
	20.600	0.090	0.56	0.11(2)	0.52(2)			$d_{aw} + bw^2$	97
WO	22.000	0.065	0.88	0.33(3)	1.150			0.27(2)w	88
	22.200	0.066	0.90	0.200	0.900	0.07ρ			85
	22.235	0.066	0.91	0.110	0.720	0.048(8)ρ			31
	31.700	0.120	0.35	0.13(2)	0.35(2)			$0.032w^2 - 0.026w$	97
	35.000	0.150	0.39	0.168[b(c)]	0.300[b(d)]	0.010ρ			91
W1	35.000	0.150	0.39	0.170	0.340	0.013(2)ρ			31
	35.000	0.150	0.39	0.100	0.250	$d_a\rho + b\rho^2$			84

	36.000	0.160	0.41	0.15(2)	0.640	$0.038(6)\rho + b\rho^2$		97
	80.000	0.450	1.37	0.5(2)	1.400			87
	90.000	0.250	1.38	0.170	0.940	$0.06(2)\rho$		31
	91.000	0.240	1.40	0.320	1.510		$0.2w + 0.06w^2$	80
W2	95.000	0.220	1.48	0.41(4)	1.500		$0.35(2)w$	88
	95.000	0.220	1.48	0.250	1.350	$d_{a\rho} + b\rho^2$		84
	110.000	0.450	2.10	0.6(2)	2.180	$0.17(3)\rho$		87
	111.000	0.470	2.20	0.97(17)	2.400		$0.45(14)w$	88
	118.000	14.110	16.45	10.000	12.000			87
	123.000	1.110	3.29	1.67(6)	3.400		$0.56(4)w$	88
W3	150.000	0.100	3.62	0.28(25)	4.000		$1.19(14)w$	88
	210.000	0.070	7.63		9.200	0.72ρ		82
	225.000	0.050	7.64	0.050	6.900	$0.54(30)\rho$		95
	230.000	0.050	7.82	1-5				83
W4	230.000	0.050	7.82	0.000	4.800	$0.37(5)\rho$		94
	240.000	0.040	8.32		7.900	0.62ρ		32
	300.000	0.020	17.40		13.400	1.05ρ		82
W5	345.000	0.010	31.00		23.000	$1.18(8)\rho$		89
	411.000		104.00		50.000	4ρ		32
	667.000				150.000	12ρ		32

[a] Digits in parenthesis give the Standard Deviation from the mean in terms of final listed digits.

[b] Tangential path: (a) x 69, (b) x 173, (c) x 53, and (d) x 142 (Ref. 91).

[c] $\rho_s = 12.8\ g/m^3$ or $w_s = 3.08$ cm and U.S. Standard Atmosphere 76.

[d] a,b - coefficient not given.

The refractivity $N_o = 40.4\rho + \delta N_o$, when measured at 40°C and 21.4 GHz and 23.6 GHz (49,56,63) exhibited also the anomalies δN_o:

RH,%	$\leq$ 85	91.0	94.0	97.0	98.0	99.0
δN_o, ppm	0	0.3	0.8	1.5	1.8	2.5

c. EWA Evidence from Field Measurements

Millimeter wave field measurements are carried out in three ways (37-101):

1. attenuation rate α (dB/km) for horizontal, line-of-sight paths;

2. total zenith attenuation A(dB); and

3. sky noise T_B(K), often employed to infer the A value.

Most of the measurements are performed at single frequencies; a few were carried out in a broadband mode (Fourier transform technique) (86,90,93,98,101). Several difficulties plague field observations:

1. absolute calibration;

2. large scatter (± 10% to ± 30%) in data due to unspecified weather along the path;

3. scarceness of data at high humidities (RH > 90%);

4. lack of simultaneous recordings of the integrated water vapor w (Eq. 33);

5. absence of data on integrated liquid water W (Eq. 49) and visibility V (Eq. 52) in cloud-free air; and

6. difficulty of fitting data empirically to surface-based meteorological variables.

Horizontal and zenith path data are summarized in Table 5 and compared with model calculations by using the U.S. Standard Atmosphere (19). As expected, the window (W1 to W5) absorption increases with the water vapor concentration ρ or path-integrated water vapor w. It was observed earlier that measurements in the 100 GHz to 117 GHz range revealed considerably higher values of water vapor absorption than were predicted by H_2O line shape theory (73).

Generally, the absorption A is divided into a dry contribution (A_d) and a wet term (A_v). The dry term is caused by oxygen absorption originating from a well-known spectroscopic data base (Section II); hence, in W1 to W3, it can serve as a check value.

The wet term determines the transparency in all window ranges. Transparency is tightly coupled to humidity [that is, ρ, w, and W(RH)] causing various propagation limitations (for example, usable range L or minimum elevation angle θ) with increasing amounts of water vapor in the path volume. A typical case exists when weather conditions change from clear and dry to cloudy and wet. The water vapor absorption problem fades rapidly away above h > 3 km. It has become a standard practice to separate the wet term into two components: one proportional with ρ (monomer), the other with a ρ^2 (dimer) dependence. The first field results to support the dimer hypothesis were taken at 220 GHz (76). Comparing these data with other available data in Table 5, one notices that in about half the cases a squared (x = 2) water vapor dependence improves the fit.

A horizontal path that operated at 182.9 GHz, close to the 183 GHz H_2O line (Table 2), exhibited differences in the water vapor proportionality depending upon clear or cloudy sky conditions. The difference, 3.9ρ compared with 4.2ρ dB/km, was reconciled when a temperature dependence of t^{10} was assumed, which is about four times the t dependence for the 183 GHz line (Eq. 29: $t^{2.3}$) (77). The same experiment produced at 171 GHz a relationship between attenuation rate ρ and concentration that becomes increasingly nonlinear when $\rho > 10$ g/m^3. Measurements in W5 (330 GHz to 360 GHz) required a linear (x = 1, y = 2.3) and squared (x = 2, y = 11) water vapor term to fit the data (89). Condensation effects were evident in recent W4 and W5 data (101). For the first time, the importance of relative humidity RH was recognized. An EWA contribution with x = 2 and y = 16 to 30 can be isolated and an increase of α_x with beginning fog conditions was measured. Predicted attenuation rates in fog are in the range 3 to 15 dB/km for ν = 100 to 300 GHz, ρ_w = 1 g/m^3 and T = 4°C (25). An independent measurement of water vapor w and liquid W contributions would be desirable.

Cumulative data taken through the total air mantle are more difficult to interpret for their phenomenological origins. In most cases, zenith attenuation A is correlated with the surface water vapor concentration ρ_o. Simultaneous measurements of the integrated vapor w, either by microwave (see Eq. 51) or infrared techniques (93) are rare. The maximum attenuation detectable in the EHF range is A $\lesssim$ 30 dB. The dry term A_d of a slanted radio path follows the secant law $A_d(90°)/\sin\Theta$, even for low angles ($\Theta \gtrsim 10°$); the wet term A_v increases very rapidly below $\Theta < 10°$ (91). A tangential path (Θ = 0) traverses about 38 times the air mass at zenith but perhaps 100 times the water vapor content.

It seems certain that A_v is a continuum spectrum (79,93,98, 108) and that earlier observations of spectral dimer features (81,86,90,64) were instrumental effects. To quote from Ref. 93:

"[EWA] shows no spectral features and scales with w." The frequency dependence of the empirical continuum spectrum (Eqs. 28 and 4) was z = 2. A fit of the A_v term between 15 GHz and 230 GHz (Table 5) yields in dB approximately

$$A_v \simeq 0.013\ \rho_o (\nu/30)^{1.7} \tag{68}$$

and the frequency dependence drops to z = 1.22 for window data taken between 140 GHz and 300 GHz (93).

Field data mostly serve the practical purpose of establishing an operational data base. Agreement with model calculations (Section II) is fair, when it is considered that the model makes use of Eq. (27) to describe the water vapor continuum. Either integrated vapor w or surface concentration ρ are useful predictors of millimeter wave window absorption (Table 5).

D. EWA Discussion

A water vapor continuum spectrum dominates the transmission behavior of atmospheric window ranges (W1 to W5: Figs. 1 to 3). Three absorption mechanisms have been parameterized to aid in identifying the respective relative contributions to the continuum. *In the course of this paper, the following picture* evolved:

	Far-wing Eq. (57)	Dimer Eq. (58)	Aero-sol Eq. (61)	Laboratory data	Field data
Relative magnitude C/C_v	1.0	EWA	EWA	2 to 10	> 2
Water vapor x	1.2	2	$\gtrsim 2$	1 + 2	1 + 2
Temperature y	3.0	8	28.0	5.5, 10, > 10, 16, 26	10, 11, 16 to 30
Frequency z	2.0	Fig. 12	0.8	1.5 to 2.5	1.2, 1.7, 2

The empirical expressions (Eqs. 62 to 68) merely organize experimental data; they are not found to be entirely satisfactory to uniquely support even one particular absorption scheme. At present it is difficult to relate EWA contributions quantitatively

to observed variables. Results vary greatly from one experiment to the next, even under controlled laboratory conditions. EWA is most prevalent when RH > 90%; however, the best type of measurement has not yet been undertaken.

There are objections to both interpretations of EWA. Unclear problems with respect to the dimer are: (a) no direct physical evidence in the atmosphere; (b) no match to the frequency-envelope of a proposed spectrum (Table 4); and (c) no unique match to the temperature dependence. A promising EWA hypothesis is, at present, the vapor-to-liquid conversion of water by aerosol particles under conditions where RH $\leq$ 100%. Here the objections lie in the fact that invisible or haze clouds (see X-distribution in Fig. 9) must exist with liquid water concentrations close to those measured in fogs or clouds (for example, RH = 96%, T = 10°C, ρ = 9, and ρ_w = 0.1 g/m^3, by using Eq. (67)). Delogne raises the point that for the case of an inhomogeneous distribution of liquid aerosol water, the visibility V is improved due to the $\rho_4^{0.6}$-dependence (Eq. 52) whereas millimeter waves respond just to the total water W (Eq. 49; Ref. 30).

Which explanation for EWA has the most merit can only be answered by additional, completely controlled experiments performed in the laboratory.

V. CONCLUDING REMARKS

The role that atmospheric water vapor plays in millimeter wave propagation was traced by means of data from modeling, laboratory, and field studies. The assumptions and approximations made, the reasoning used, the relative importance of various parameters, the limitations of available data, and the separation of water vapor and liquid water effects have been addressed. Molecular absorption due to oxygen is prominent in the 45 GHz to 125 GHz range (Fig. 3); water vapor dominates at higher frequencies, actually up to 30 THz (Figs. 1 and 2). Considering only molecular absorbers (H_2O and O_2) for a cloudless atmosphere leads invariably to discrepancies between predicted and measured attenuation rates. The problem is most apparent in the EHF window ranges. A horizontal path at sea level can experience, at 220 GHz for example, the following varying attenuation rates (32):

Clear air	1.6 to 11.2 dB/km
Fog	0.4 to 4.7 dB/km
Rain (< 10 mm/hr)	1 to 7 dB/km

These values demonstrate the relative importance of understanding the clear air problem first. Clear air attenuation is related to atmospheric water vapor content; unfortunately, more than

two-thirds of this contribution is described only by empirical formulas that lack both physical insight and general applicability.

A reasonably concise model for the molecular absorption was presented in Section II and then applied to identify the magnitude and frequency and physical dependencies of the non-H_2O contribution to the available data body reported for laboratory and field experiments. The contribution is called EWA (excess water vapor absorption) and it was found the EWA exhibits in the millimeter wave range a continuum spectrum similar in frequency response to the dielectric loss spectrum of water. The search for liquid water in clear air led to the water-uptake phenomenon of aerosol particles, which grow rapidly in moist air with increasing RH. This problem has been addressed in the infrared (9,20,23) and deserves further study with respect to influences on millimeter waves.

Most of the evidence found in parameterizing EWA data supports a condensation phenomenon driven by relative humidity, RH: (a) the nonlinear pressure dependence (aerosol growth function), (b) the strong negative temperature dependence, (c) hysteresis effects when cycling the RH, (d) the governing variable is relative (RH) and not absolute (ρ) humidity, and (e) the failure of molecular approaches hypothesizing weakly bonded dimers but neither matching the spectral response nor the temperature dependence and number concentration necessary.

From a practical point of view, one is looking for invisible liquid water content in the range $W \simeq 0.02$ to 0.2 mm when $RH \leq 100\%$, which are normally known to exist under haze, cloud and fog conditions. But clouds and fog imply only larger, optically active ($r > 1$ μm) particle sizes. Should the condensation hypothesis have merit, then EWA can serve as a tracer to the otherwise not directly accessible world of atmospheric submicron particles. A systematic EWA study under controlled laboratory conditions of high humidity (RH = 90% to 99.9%) could reveal growth functions for particular aerosol ensembles and elucidate the various stages and time scales that H_2O molecules undergo in moist air until they become barely visible as clusters of $> 10^9$ molecules.

SYMBOLS AND ACRONYMS

Acronyms

AFGL	Air Force Geophysical Laboratory
CM	condensation nuclei
CCN	cloud condensation nuclei

D1-D4	O_2-MS doublets (Table 1)
EWA	excess water vapor absorption
E18	computer short-form for 10^{18}
EHF	extreme high frequency range (30 to 300 GHz)
HITRAN	high resolution transmission model developed by AFGL
H-bond	molecular hydrogen bond
ID	quantum number identification
IM	imaginary part of
O_2-MS	oxygen microwave spectrum
RE	real part of
W1-W7	atmospheric transmission windows

Wymbols

a	*coefficient for fitting* $\propto \rho$, Tabel 5
a_1-a_5	O_2-MS line coefficients, Eqs. (21) to (23) and Table 1
A	total attenuation, Eq. (6), dB
b	*coefficient for fitting data* $\propto \rho^2$, Table 5
b_1-b_3	H_2O line coefficients, Eqs. (24) and (25), Table 2
B(t)	second virial coefficient, Eq. (37) m^3
c	speed of light, Eq. (3), km/s
C	continuum magnitude, Eq. (53)
d	molecular spacing, Section III, m
$D(\nu)$	*dispersion spectrum, Eq. (13), ppm*
e	water vapor pressure, Eq. (11), kpa
E	field strength, Eq. (2), V/m
f	relative humidity RH, Eq. (45), 1
F'	line shape for $D(\nu)$, Eq. (15), GHz^{-1}
F"	line shape for $N"(\nu)$, Eq. (16), GHz^{-1}
g(f)	aerosol mass growth factor, Eq. (47), 1
h	altitude, Eq. (32), km
i	running spectral line index, Tables 1 and 2
I	interference coefficient, Eq. (23), 1
j	$= \sqrt{-1}$, Eqs. (1) and (3)
k(t)	dimer equilibrium factor, Eq. (39), m^{-3}
ℓ	mean free path length, Section III, μm
L	radio path length, Eq. (2), km
m	molecular mass, Eq. (20)
M	molecular number density, Eq. (36), molec/m^3
n	refractive index, Fig. 13, 1
n'	real part of n, Eq. (58), 1
n"	imaginary part of n, Fig. 13, 1
N	complex refractivity, Eq. (1), ppm
N_o	frequency-independent part of N, Eq. (12), ppm
$N'(\nu)$	refraction spectrum, Eq. (27), ppm
$N"(\nu)$	absorption spectrum, Eq. (14), ppm
P	dry air pressure, Eq. (12), kPa
δp	fluctuations of p, Eq. (34), kPa
Q	resonator quality factor, Table 3, 1

r	aerosol particle radius, Eq. (35), μm
RH	relative humidity, Eq. (45), %
s	ray path length, Eq. (6), km
s_1, s_2	ray path coordinate, Eqs. (6) and (8)
ds	path length increment, Eq. (6), km
S	line strength, Eqs. (21) and (24), kHz
S_A	aerosol surface area, Eq. (46), cm^2
t	300/T, normalized inverse T, Eq. (11), 1
T	temperature, Eq. (11), K
T_B	brightness temperature, Eq. (10), K
V	visibility, Eq. (52), km
V_v	air volume containing water vapor, Section IV, cm^3
w	total precipitable water vapor, Eq. (33), cm
W	total precipitable liquid water, Eq. (49), mm
x	concentration exponent (ρ), Eq. (53)
y	temperature exponent (t), Eq. (53)
z	frequency exponent (ν), Eq. (53)
α	attenuation rate, Eq. (4), dB/km
γ	line width, Eq. (22), GHz
γ_D	Doppler line width, Eq. (20), kHz
Γ	propagation constant, Eq. (3), 1
ε	deviation from ideal gas behavior, Eq. (38), 1
η	propagation delay time, Eq. (9), ns
η_{Ad}	time constant for adsorption, Section IV.*B.*, s
η_{De}	time constant for desorption, Section IV,*B.*, s
θ	slant path angle, Section II, degree
λ	optical wavelength, Section III, m
ν	frequency, Eq. (3), GHz
ν_o	line resonance frequency, Eq. (15), GHz
ρ	water vapor concentration, Eq. (36), g/m^3
$\bar{\rho}$	path-averaged value of ρ, Eq. (52), g/m^3
δρ	fluctuations of p, Eq. (34), g/m^3
τ	transmittance, Eq. (7), 1
φ	phase rate, Eq. (5), rad/km
Ø	total phase delay, Eq. (8), rad
Σ	sum of, Eqs. (13) and (14)

Subscripts

A	aerosol
D	dimer
d	dry
ℓ	absorption line
L	Lorentzian
m	maximum
n	integer, cluster size
o	initial value
s	saturation
v	water vapor
w	liquid water

x EWA
μ optical wavelength (λ = 0.55 μm)

REFERENCES

Atmospheric Attenuation, Refraction, Dispersion, and Emission

1. Van Vleck, J. H., *Phys. Rev. 71*, 425-433 (1947).
2. Birnbaum, G., *J. Chem. Phys. 21*, 57-61 (1953.
3. Zhevakin, S. A., and Naumov, A. P., *Izv. Vysshikh Uchebn, Zavedenii, Radiofiz. 6*, 674-695 (1963) (Russian transl.).
4. Hall, J. T., *Appl. Optics, 6(8)*, 1391-1398 (1967); also *in* "Proc. Sym. on Sub-MM Waves," pp. 455-465, Polytechn. Inst., Brooklyn, New York (1970).
5. Zhevakin, S. A., and Naumov, A. P., *Radio Engrg. Electronic Phys. 12*, 885-894, 1067-1076 (1967) (Russian trans.).
6. Viktorova, A. A., and Zhevakin, S. A., *Soviet Phys. Doklady, 11*, 1059-1068 (1967) (Russian transl.).
7. Liebe, H. J., *IEEE Trans. AP-17*, 621-627 (1969).
8. Viktorova, A. A., and Zhevakin, S. A., *Sov. Phys.-Kokl. 15(9)*, 836-855 (1971).
9. Hodges, J. A., *Appl. Optics, 11(10)*, 2304-2310 (1972).
10. McClatchey, R. A., Benedict, W. S., Clough, S. A., Burch, D. E., Calfee, R. F., Fox, K., Rothman, L. S., and Garing, J. S., AFCRL Atmospheric Absorption Line Parameters Compilation, AFCRL Environm. Research Paper, No. 434 (1973); revisions in: *Appl. Optics, 15*, 2616 (1976); *17*, 507; *17*, 3517-3518 (1978).
11. Gaut, N. E., and Reifenstein, E. C. III, Environmental Research and Technology, Inc., Tech. Rpt. 75-0-1949 (1975).
12. Roberts, R. E., Selby, J. A., and Biberman, L. M., *Appl. Optics, 15(9)*, 2085-2090 (1976).
13. Lam, K. S., *J.Q.S.R.T. 17*, 351-383 (1977).
14. Derr, V. E., and Calfee, R. F., Spectral Transmission of Water Vapor from 1 to 1200 cm^{-1} at Low Concentration and Low Pressure, NOAA Tech. Memo ERL WPL-24 (July 1977).
15. Liebe, H. J., Gimmestad, G. G., and Hopponen, J., *IEEE AP-25(3)*, 327-335 (1977).
16. McMillan, R. W., Gallagher, J. J., and Cook, A. M., *IEEE MTT-25(6)*, 484-488 (1977).

17. Liebe, H. J., and Gimmestad, G. G., *Radio Science, 13(2)*, 245-251 (1978).

18. Montgomery, G. P., Jr., *Appl. Optics, 17(15)*, 2299-2303 (1978).

19. Liebe, H. J., and Rosich, R. K., Modeling of EHF Propagation in Clear Air, Proc. IEEE Conf. Space Instrum. for Atm. Observation, El Paso, Texas, pp. 5/1-15 (IEEE Catalog No. 79 Ch 1380-5 REG 5) (April 1979); also, AGARD CP 238-II, 45/1-18 (1978).

20. Tam, W. G., and Boily, C., *Infrared Phys. 19*, 151-162 (1979).

21. Suck, S. H., Kassner, J. L., Jr., and Yamaguchi, Y., *Appl. Optics, 18(15)*, 2609-2617 (1979).

22. Carlon, H. R., *Infrared Phys. 19*, 549-557 (1979).

23. Nilsson, B., *Appl. Optics, 18(20)*, 3457-3473 (1979).

24. Burch, D. E., and Clough, S. A., *in* "Near-Millimeter Wave Technology Base Study, Vol. 1" (S. M. Kulpa and E. A. Brown, eds.), DARPA Report HDL-SR-79-8 (U.S. Army MDRC) (November 1979).

25. Falcone, V. J., Jr., Abreu, L. W., and Shettle, E. P., Atmospheric Attenuation of Millimeter and Submillimeter Waves: Models and Computer Code, U.S. Air Force Geophysics Lab., Tech. Report AFGL-TR-79-0253 (Environm. Research Paper 679) (October 1979).

26. Cutten, D. R., *Infrared Phys. 19*, 663-667 (1979).

27. Pinnick, R. G., Jennings, S. G., Chylek, P., and Auvermann, H. J., *J. Atmos. Sci. 36*, 1577-1586 (1979).

28. Carlon, H. R., and Harden, C. S., *Appl. Optics, 19(11)*, 1776-1786 (1980).

29. Smith, H. J., Dube, D. J., Gardner, M. E., Clough, S. A., Kneizys, F. X., and Rothman, R. S., FASCODE--Fast Atmospheric Signature Code, U.S. Air Force Geophysics Lab., Tech. Report AFGL-TR-78-0081 (January 1978).

30. Delogne, P., Attenuation of Millimetric and Visible Waves by Aerosols, Open Symposium Preprein, A2.1 (May 1980) (URSI-F, Internat. Symp., Lennoxiville, Canada).

Comprehensive Treatments

31. Waters, J. R., *in* "Methods of Experimental Physics, Vol. 12B" (M. L. Meeks, ed.), Chapter 2.3, Academic Press, New York (1976).

32. Kulpa, S. M., and Brown, E. A., Near-Millimeter Wave Technology Base Study, DARPA Report HDL-SR-79-8 (U.S. Army MDRC), Vol. 1 (November 1979).

33. McCartney, E. J., "Optics of the Atmosphere: Scattering by Molecules and Particles," Wiley, New York (1976).

Selected Properties of Atmospheric Water

34. Yue, G. K., *J. Aerosol Sci. 10,* 75-86 (1979).

35. Hänel, G., *in* "Advances in Geophysics, Vol. 19," pp. 74-188, Academic Press, New York (1976).

36. Shettle, E. P., and Fenn, R. W., Models for the Aerosols of the Lower Atmosphere and the Effects of Humidity Variations on Their Optical Properties, U.S. Air Force Geophysics Lab., Tech. Report AFGL-TR-0214 (September 1979).

37. Turner, R. E., Gebhardt, F. G., Manning, J. L., Meredith, R. E., Singer, S. M., and Vavra, P. C., Model Development for E-O SAEL: Natural Aerosol, Contrast, Laser Transmission, and Turbulence, U.S. Army ERDC, Atmospheric Sciences Lab. Report ASL-CR-80-0127-1 (January 1980).

38. National Academy of Sciences, Airborne Particles, Report by Subcommittee, Div. Medical Sciences, University Park Press, Baltimore, Maryland (1979).

39. Liou, K. N., and Duff, A. D., *J. Appl. Met. 18,* 99-103 (1979).

40. Guiraud, F. O., Howard, J., and Hogg, D. C., *IEEE Trans. GE-17(4),* 129-136 (1979); also, Data Report on Measurements of Precipitable Water Vapor and Cloud Liquid at Fort Sill, 1979, NOAA-Data Report ERL WPL-2 (October 1979).

41. Pruppacher, H. R., and Klett, J. D., "Microphysics of Clouds," Reidel Publishing, Boston, Massachusetts (1978).

42. Barrett, E. W., Parungo, F. P., and Pueschel, R. F., *Meteorol. Resch. 32,* 136-149 (1979).

43. Dyke, T. R., Mack, K. M., and Muenter, J. S., *J. Chem. Phys. 66(2),* 498-510 (1977).

44. Curtiss, L. A., Fruip, D. J., and Blander, M., *J. Chem. Phys. 71(6),* 2703-2711 (1979).

45. Ferguson, E. E., Fehsenfeld, F. C., and Albritton, D. L., *in* "Gas Phase Ion Chemistry, Vol. 1," pp. 45-81, Academic Press, New York (1979).

Laboratory Measurements

46. Becker, E. G., and Autler, S. H., *Phys. Rev. 70(5,6)*, 300-307 (1946).

47. Froome, K. D., *Proc. Phys. Soc. (London), B-68*, 833-835 (1955).

48. Bourdouris, G., *J. Res. NBS, 67D(6)*, 631-684 (1963).

49. Liebe, H. J., Untersuchungen an Gasmischungen, insbesondere Wasserdampf-Luft, Mit einem digitalen Mikrowellen-Refraktometer, Ph.D. Thesis, Techn. University, West Berlin, Electrical Dept. (D83) (1964); also, *NTZ Communications J. 19*, 79-83 (1966) (in German).

50. Newell, A. C., and Baird, R. C., *J. Appl. Phys. 36*, 79-83 (1965).

51. Rusk, J. R., *J. Chem. Phys. 42(2)*, 493-494 (1965).

52. Hay, D. R., and Turner, H. E., *in* "Humidity and Moisture, Vol. 2" (A. Wexler, ed.), pp. 611-615, Reinhold Publishing, New York (1965).

53. Frenkel, L., and Woods, D., *Proc. IEEE, 54(4)*, 498-505 (1966).

54. Burch, D. E., *J. Opt. Soc. Am. 58*, 1383-1394 (1968).

55. Hemmi, C. O., and Straiton, A. W., *Radio Sci. 4(1)*, 9-15 (1969).

56. Mrowinski, D., Refraktion und Absorption in atmosphärischen Gasen in der Umgebung der 22 GHz H_2O Linie, Ph.D. Thesis, Techn. University, West Berlin, Germany, Electr. Eng. Dept. (1969); also, Angew, Z., *Phys. 29(5)*, 323-330 (1970) (in German).

57. Liebe, H. J., and Dillon, T. A., *J. Chem. Phys. 50*, 727-732 (1969).

58. Harries, J. E., Burroughs, W. J., and Gebbie, H. A., *J.O.S.R.T. 9*, 799-807 (1969); also, Burroughs, W. J., Jones, R. G., and Gebbie, H. A., *J.Q.S.R.T. 9*, 809-824 (1969).

59. Sheppard, A. P., Breeden, K. H., and McSweeney, A., *in* "Proc. Sym. on Sub-Waves," pp. 445-453, Polytechn. Inst. Brooklyn, New York (1970).

60. Bignell, K. J., *Quant. J. Roy. Met. Soc. 96*, 390-403 (1970).

61. Burch, D., Gryvnak, D., and Pembrook, J., Jr., Continuous Absorption in the 8-4 μm Range by Atmospheric Gases, Philco-Ford Report F19 628-69-C-0263 (1971).

62. Straiton, A. W., Fannin, B. M., and Perry, J. W., *IEEE Trans. AP-22(4)*, 613-616 (1974).

63. Liebe, H. J., Studies of Oxygen and Water Vapor Microwave Spectra under Simulated Atmospheric Conditions, OT Rpt. 75-66, U.S. Government Printing Office, Washington, D.C. (June 1975).

64. Llewellyn-Jones, D., Knight, R. J., and Gebbie, H. A., *J. Phys. E: Sc. Instr. 9*, 690-692 (1976).

65. Gimmestad, G. G., An Experimental Study of the Oxygen Microwave Spectrum, Ph.D. Thesis, Dept. Phys. & Astrophys., University of Colorado (1978).

66. Llewellyn-Jones, D. T., Knight, R. J., and Gebbie, H. A., *Nature, 274(5674)*, 876-878 (1978).

67. Kemp, A. J., Birch, J. R., and Afsar, M. N., *Infrared Phys. 18*, 827-833 (1978).

68. White, K. O., Watkins, W. R., Bruce, C. W., Meredith, R. E., and Smith, F. G., *Appl. Optics, 17(17)*, 2711-2720 (1978).

69. Bohlander, R. A., Spectroscopy of Water Vapor, Ph.D. Thesis, Dept. Physics, Imperial College, London (1979).

70. Peterson, J. C., Thomas, M. E., Nordstrom, R. J., Damon, E. K., and Long, R. K., *Appl. Opt. 18(6)*, 834-841 (1979).

71. Watkins, W. R., White, K. O., Bower, L. R., and Sojka, B. Z., *Appl. Opt. 19(8)*, 1149-1160 (1979).

72. Jona, M., *Physik. Zeitschr. 20*, 14-21 (1919) (in German).

Field Measurements

73. Crawford, A. B., and Hogg, D. C., *Bell Syst. Tech. J. 35*, 907-916 (1956); also, Hogg, D. C., *J. Appl. Phys. 30(9)*, 1417-1419 (1959).

74. Tolbert, C. W., Krause, L. C., and Straiton, A. W., *J. Geophys. Res. 69(7)*, 1349-1357 (1964).

75. Chang, S. Y., and Lester, J. D., *IEEE Trans. AP-16(5)*, 588-591 (1968).

76. Malyshenko, Y. I., *Rad. Eng. & Electr. Phys. 14(3)*, 447-450 (1969) (Russian transl.).

77. Whaley, T. W., Characterization of Free Space Propagation Near the 183 GHz H_2O Line, Ph.D. Thesis, U. of Texas, Electr. Eng. Dept. (1968); also, *IEEE Trans. AP-17(5)*, 682-684 (1969).

78. Wrixon, G. T., *Bell Sys. Tech. J. 50(1)*, 103-114 (1971).

79. Mather, J. C., Werner, M. W., and Richards, P. L., *Astrophys. J. 170,* L59-65 (1971).

80. Thompson, W. I. III, Atmospheric Transmission Handbook, NASA Tech. Rept. No. DOD-TSC-NASA-71-6, Chapter 9 (1971).

81. Gibbins, C. J., *Nature, 243,* 397 (1973).

82. Ulaby, F. T., *IEEE Trans. AP-21(2),* 2666-2669 (1973).

83. Goldsmith, P. F., Plambeck, R. L., and Chiao, R. Y., *IEEE Trans. MTT22(12),* 1115-1116 (1974).

84. Lo, L. I., Fannin, B. M., and Straiton, A. W., *IEEE Trans. AP-23(6),* 782-786 (1975).

85. Fogarty, W. G., *IEEE Trans. AP-23(3),* 441-444 (1975).

86. Emery, R. J., Moffat, P., Bohlander, R., and Gebbie, H. G., *J. Atm. Terrestr. Phys. 37,* 587-594 (1975).

87. Gibbins, C. J., Gordon-Smith, A. C., and Croom, D. L., *Planet. Space Sci. 23,* 61-73 (1975).

88. Gibbins, C. J., Wrench, C. L., and Croom, D. L., Atmospheric Emission Measurements between 22 and 150 GHz, Proc. URSI Comm. F Sym., LaBaule, France (1976).

89. Ryadov, V. Y., and Furashov, N. I., *Radio Phys. & Quant. Electr. 19,* 918-922 (1977) (Russian transl.).

90. Moffat, R. H., Bohlander, R. A., Macrae, W. R., and Gebbie, H. A., *Nature, 269,* 676-677 (1977).

91. Altshuler, E. E., Gallop, M. A., and Telford, L. E., *Radio Sci. 13(5),* 839-852 (1978).

92. Zabolotniy, V. F., Iskhakov, I. A., Sokolov, A. V., and Sukhonin, E. V., *Infrared Phys. 18,* 815-817 (1978).

93. Hills, R. E., Webster, A. S., Alston, D. A., Morse, P. L., Zammit, C. C., Martin, D. H., Rice, P. C., and Robson, E. I., *Infrared Phys. 18,* 819-825 (1978).

94. Wrixon, G. T., and McMillan, R. W., *IEEE Trans. MTT-26(6),* 434-439 (1978).

95. Plambeck, R. L., *IEEE Trans. AP-26,* 737-738 (1978).

96. Robson, E. I., and Rowan-Robinson, M., *Infrared Phys. 19,* 115-120 (1979).

97. Hogg, D. C., and Guiraud, F. O., *Nature, 279(5712),* 408-409 (1979).

98. Rice, D. P., and Ade, R. A., *Infrared Phys. 19,* 575-584 (1979).

99. Ho, K. L., Mavrokoukoulakis, N. D., and Cole, R. S., *Microwave Opt. Acoust. 3(3),* 93-98 (1979).

100. Tanton, G. A., Mitra, S. S., Stettler, J. D., Morgan, R. L., Osmundsen, J. F., and Castle, J. G., Near Ground Attenuation of 0.89 mm Radiation, Proc. 4th Mt. Conf. Infrared & MM-Waves (IEEE Cat. 79 CH 1384-7 MTT), 27 (December 1979).

101. Emery, R. J., and Zavody, A. M., *Radio Elect. Eng. 49*, 370-380 (1979).

Refractive Index of Water

102. Pottel, R., *in* "Water--A Comprehensive Treatise, Vol 1: The Physics and Physical Chemistry of Water" (F. Franks, ed.), Chapter 7, Plenum Press, New York (1972).

103. Ray, P. S., *Appl. Opt. 11(8)*, 1836-1844 (1972).

104. Afsar, M. N., and Hasted, J. B., *J. Opt. Soc. Am. 67(7)*, 902-904 (1977).

105. Afsar, M. N., and Hasted, J. B., *Infrared Phys. 18*, 835-841 (1978).

106. Simpson, O. A., Bean, B. L., and Perkowitz, S., For Infrared Optical Constants of Liquid Water Measured with an Optically Pumped Laser, *J. Opt. Soc. Am. 70* (1980).

Instrumentation

107. Gerber, H. E., Saturation Hygrometer for the Measurement of Relative Humidity between 95 and 105%, *J. Appl. Meteorology* (1980).

Additional References

108. Crane, R., Attenuation Estimates for Millimeter Wave Windows near 94, 140, and 220 GHz, ERT Document T-A-502 (May 1980) (available from Environm. Res. and Techn. Inc. Concord, Massachusetts 01742).

109. Bohlander, R. A., Emery, R. J., Llewellyn-Jones, D. T., Gimmestad, G. G., and Gebbie, H. A., *in* "Proc. Workshop MM and SubMM Atmospheric Propagation" (O. Essenwanger and D. Stewart, eds.), pp. 57-66, U.S. Army Missile Command Tech. Report RR-80-3 (February 1980).

110. Poynter, R. L., and Pickett, H. M., Submillimeter, Millimeter, and Microwave Spectral Line Catalogue, JPL (Jet Propulsion Lab., NASA, Pasadena, California 91103) Publication 80-23 (June 1980).